7-2015

Functional analysis of the MMS19 gene in Carica papaya

Jorge A. Trujillo
University of Texas-Pan American

FUNCTIONAL ANALYSIS OF THE MMS19 GENE IN CARICA PAPAYA

A Thesis

by

JORGE A. TRUJILLO

Submitted to the Graduate School of
The University of Texas-Pan American
In partial fulfillment of the requirements for the degree of

MASTER OF SCIENCE

July 2015

Major Subject: Biology

FUNCTIONAL ANALYSIS OF THE MMS19 GENE IN CARICA PAPAYA

A Thesis
by
JORGE A. TRUJILLO

COMMITTEE MEMBERS

Dr. Anxiu Kuang
Chair of Committee

Dr. Qingyi Yu
Co-chair of Committee

Dr. Luis Materon
Committee Member

Dr. Richard Gilkerson
Committee Member

July 2015

ABSTRACT

Trujillo, Jorge A., Functional Analysis of the MMS19 Gene in Carica papaya. Master of Science (MS), July 2015, 78 pp., 2 tables, 26 figures, 57 references, 57 titles.

All organisms face DNA-damaging radiation in the form of UV light and must have mechanisms to repair or undo damage. Plants being stationary organisms must cope with damaging UV rays in a molecular fashion and so have developed many forms of resistance. *MMS19* is implicated in DNA repair indirectly as a nuclear encoded gene that binds onto protein assembly complexes in the cytosol. A mutant within the SunUp variety of *Carica papaya* has a large deletion for *MMS19* and presents a diminutive phenotype. Deficient DNA repair mechanisms will shunt cells out of the natural cell cycle and reduce cell proliferation and differentiation. In this study the diminutive phenotype was characterized using electron microscopy, fluorescent microscopy, and RT-PCR. Mutant cells within leaf tissues showed increased autolytic and apoptotic activity, reduced expression of downstream genes indicating that MMS19 is necessary for maintaining normal growth and development of papaya.

DEDICATION

I dedicate the completion of this Master's degree to my family who supported me throughout this transformative journey. I would like to thank my father for pushing me to complete my manuscript every day and my mother for her enthusiasm and interest in my research.

I also want to thank all of my friends and collaborators who cheered me on to finish this work and assisted in the creation of this manuscript.

Lastly I would like to thank my faculty advisors for teaching me all the valuable skills I have learned. I will carry all these experiences with me throughout my career and teach the same form of excellence you all inspired in me to others.

AKNOWLEDGEMENTS

This manuscript is a compilation of several years of research that would not have been successful without the help of my faculty mentors and research peers both from UTPA and AgriLife Texas A&M University. I am especially indebted to Dr. Qingyi Yu for offering me a position in her research lab to begin investigation into this project. I am forever grateful to Dr. Anxiu Kuang who agreed to conduct this joint research project and welcomed me most graciously into her own research lab.

The research conducted during my internship at AgriLife Dallas would not have been possible without a grant from the National Science Foundation. It was through this summer internship that my apprehension and skills for molecular lab work increased profoundly. A great mentor during this internship, Dr. Ratnesh Singh was always offering helpful advice and walkthroughs in both technical skills and bioinformatics. My completion of qPCR would not have been as complete without his help. I am extremely thankful to my mentor Dr. Kuang who helped me visualize my project one step at a time and inspired me to present my research at conferences. I would also like to thank Dr. Materon for mentorship in bettering my biological writing and inspiring me through his virology course. I'd like to thank Dr. Gilkerson for offering ideas on quantifying cell size and help in fluorescent microscopy. I am also thankful to Dr. Daniel Plas and his laboratory for assistance in confocal microscopy and immunogold labeling.

Lastly I would like to acknowledge the entire graduate faculty and students who helped garner a sense of community within our department.

TABLE OF CONTENTS

LIST OF TABLES

LIST OF FIGURES

CHAPTER I

INTRODUCTION

Statement of Problem

Commonly referred to as the papaya tree, *Carica papaya* (L.) is a species of tropical herb well known for its large palmate leaves. A single fully expanded leaf on a mature plant may reach a width of 30-60 cm (Morton, 1987). These large sizes in foliage as well as the large height (6-9 m) of the plant indicate a demand for robust growth. A typical fruit for a papaya plant measures anywhere from 15-50 cm and comes in a variety of forms. Fruit can weigh up to 9 kg-s and ripens to a yellow, orange, or salmon red color along with a distinct aroma. Because of its tropical origins, papaya is a perennial plant. Papaya can go from seed to fruit in less than 11 months depending on climate. All these characteristics of the plant contribute to its remarkable adaptability to climates around the world. Modern cultivation of the plant has produced many varieties to suit different growing conditions as well as consumer preferences.

Papaya is an economically important crop that is grown worldwide and has substantial nutritive value (Ming, 2008). Original cultivation is hypothesized to have occurred in southern Mexico to Central America by pre-classical Mesoamericans. Rapid colonization of the Americas resulted in exportation of papaya seeds to world markets. Papaya plant is now considered to be naturalized to many parts of the world including the Bahamas, Puerto Rico, and Hawaii.

Economically significant production areas include Hawaii, tropical Africa, Australia, Philippines and India. Most production before the 20th century consisted of small commercial scale growers meeting local demands. Some importation of unique varieties began in the 1950's. As global markets began to increase the transportation of crops, pests would stowaway along with these foodstuffs and invade new populations in otherwise undisturbed habitats. In this papaya was extraordinarily susceptible to pestilence with few natural defenses. Fruit flies, white flies, and web worms are a few of the insect pests that lay eggs in fruit or cover leaves with honeydew. These pests easily spread in a population and can devastate an entire crop in a single season. Aside from the devastating effects these pests wreak on papaya plants, the proliferation of mosaic and ring spot viruses is equally damaging to a crop. Mechanically transmitted by either the grower's handling of infected plants or the transmission through leaf borer insects, these viruses spread quickly. Once infected a plant has little success in response to the disease and cannot be treated as there is no cure. Infected plants are either isolated or designated for destruction due to infection. Pesticides are normally the method of treatment in an attempt to rid the field of the transmitting agent, which is usually an aphid of the species *Myzus persicae* or *Aphis spiraecola*. In states like Hawaii, isolation from the mainland reduced the effects of plant viruses on papaya plantations. With increasing globalization of trade, the inevitable crossover of insects carrying these diseases arrived on the island and quickly became a problem for the native growers (Agriculture 2000). Farmers discovered PRSV on the island of Puna in 1992. Shortly after the Hawaiian papaya industry began to decline in production due to massive infections (Agriculture 2000). The Department of Agriculture in Hawaii was tasked with containment of the disease and efforts concentrated largely on removing infected plants and destroying them. Virus resistant strains were implemented by farmers attempting to combat the scourge of the

PRSV by planting them alongside traditional strains. Albeit these attempts the disease continued to spread on the islands of Hawaii. A small task force was created by the Hawaii Department of Agriculture to begin the process of generating transgenic varieties of papaya that would be immune to PRSV. A resistant line was bred from the variety 'Sunset' and given the name 'SunUp'. This transgenic papaya was then bred with a 'Kapoho' variety to produce the desirable flesh color and fruiting characteristics favored by Hawaiian farmers. Field trials began in the early 1990's to test the efficacy of this new transgenic variety. Results quickly showed that the insertion of the ring spot virus coat protein into the papaya's genome resulted in auto-immunity to infection by the virus. The now commercially viable and widespread Rainbow variety of transgenic papaya has become widely planted and has helped fight off PRSV successfully.

With recent advances in DNA sequencing technology and affordability, many organisms have had their genomes sequenced and mapped successfully. Of the flowering plants, papaya's draft genome was published in 2008 and is "the first commercial virus-resistant transgenic fruit tree to be sequenced" (Ming, 2008). These features give papaya a high attractiveness for functional genomics and bioinformatics. A diminutive mutant was identified in a population of SunUp transgenic papayas by its stunted growth, diminutive stature and reduced fertility (Yu 2014). Papaya growers worldwide depend on the cycling and replanting of new trees to meet the high demand for production of papaya. Most varieties of papaya will decrease their fruit productivity after a set number of years (~ 5 years). This in turn forces growers to identify longer living varieties that have more peak productivity. Because the MMS19 pathway is associated with telomere maintenance and growth, knowledge of how this gene functions within papaya is critical.

An F2 mapping population was developed to characterize the mutant phenotype of the diminutive plant by researchers at AgriLife Research Weslaco. Physical map of the papaya genome revealed a 36.8 kb deletion within the diminutive mutant. This large deletion occurred within the putative MMS19 homolog of *Carica papaya*. This gene has been cited in many studies to be involved in maintaining adequate DNA repair in eukaryotes as well as telomere maintenance, transcription, and DNA replication (Hatfield, 2006).

Statement of Purpose

Functional genomics seeks to identify and characterize genes and the proteins they produce within cells. With the abundance of molecular sequencing and genomic databases readily available, this area of biology is now undergoing rapid development. Scientists are able to study the function of genes through the creation of "knock-down" mutants. These are organisms that have had genomes altered in a way so as to decrease the expression of mRNA or functional protein for a specific gene(s). Once the gene of interest has been silenced, any observable phenotypical changes are studied and attributed where necessary. Various methods exist to decrease the expression profile of a gene artificially. Many of these are time consuming to perfect and costly to the researcher. In the case of the transgenic SunUp variety of papaya studied here, the large deletion of the MMS19 gene results in a non-functional or pseudo-functional protein product that in turn produces the diminutive phenotype. Whether this mutation directly affects the organism's appearance or instead has a cumulative effect over time remained to be elucidated. With tissues ready to be sampled and studied, functional analysis of the MMS19 gene could begin immediately.

MMS19 has been widely studied in yeast and animals. The gene is well described in medical literature and has unique congenital diseases associated with it (Matsuno, 2007). The

primary characteristic of this gene deficiency is the inability to repair DNA upon damage. The gene has also been implicated to be involved in telomere maintenance and transcription. Although this gene is well conserved across Eukarya, very few studies have been conducted on plants.

It was hypothesized that the large deletion of the MMS19 gene in *Carica papaya* was responsible for the diminutive phenotype exhibited by the organism. In order to confirm this association, microstructural analysis of cells within tissues as well as molecular analysis of gene expression profiles would be conducted by the researcher. Tissues were fixed and processed for observation under electron microscope. Comparisons were made between the diminutive MMS19 mutant and a wild type control. Light microscopy was employed to assess the overall structural differences in leaves and flowers. Electron microscopy was used to describe the microstructural differences observed within different layers of cells and organelles. Scanning electron microscopy showed some of the differences notable for the mutant type in the exterior of the plant. Molecular tests used to analyze the expression patterns of MMS19 included PCR, semi-quantitative PCR, and real-time PCR. Several databases were used to identify orthologous genes of interest that might be affected by the MMS19 mutation within the mutant. Expression profiles were created for these genes and described using the Pfaffl equation.

Cell viability assays were conducted using Hoechst stains to visualize stable DNA within nuclei of leaf cells. Confocal microscopy was used to capture images of these leaves and quantified for fluorescence. A polyclonal antibody against the MMS19 protein was used to localize the gene expression in tissues and the results of immunolabeling in thin sections were interpreted under Transmission Electron Microscopy (TEM).

CHAPTER II

REVIEW OF LITERATURE

Characterization of MMS19 in yeast

MMS19 was originally characterized in the yeast *Saccharomyces cerevisiae* in the late 1970's (Prakash, 1977). Over the last three decades research into the expression and function of this gene has provided a strong understanding of various biochemical interactions and molecular pathways surrounding the repair and revitalization of DNA. A gene that is well expressed throughout the life cycle of the cell, MMS19 is indispensable in many higher order organisms such as rats and humans. Amongst simpler unicellular life MMS19 mutants exhibit various characteristic deficiencies of growth and sensitivities to DNA damaging agents (Queimado, 2001).

Sensitivity to DNA damaging agents

The *MMS19* gene was first identified in a study on yeast that sought to isolate mutants that had sensitivity to alkylating agents (Prakash 1977). Those mutants that showed severe impairment in growth and development *in vitro* were labeled with a variety of different RAD (radiation deficient) names. *MMS19* was isolated as a yeast mutant that not only suffered damage by UV radiation but could not repair nicks in DNA that contained interstrand crosslinks caused by chemical damage. The chemical used in these experiments was an alkylating agent known as

methyl methanesulfonate (MMS), a known carcinogen and reproductive toxicant (Scorecard). Cells that showed a deficiency when exposed to this agent would be unable to repair the damage caused to DNA by MMS. The biochemical action of MMS is to methylate nucleotides in DNA that will in turn halt replication forks from proceeding (Prakash 1977). Simple methyltransferases, base excision repair pathway, and homologous recombination normally suffice in repairing these forms of damage. However when a cell is overwhelmed by a high concentration of alkylating chemical such as MMS, numerous covalent modifications will become more difficult to repair. It is hypothesized that during DNA replication, the replication fork will encounter one of these covalently linked nucleotides and cause a single strand break (SSB). If unrepaired this type of damage could lead to genome instability and chromosomal aberrations (Pascucci 2004). Any deficiency such as a mutation that would occur in the repair mechanisms that undo this type of damage will confer sensitivity to MMS.

The original screens that tested for these MMS sensitive mutants also showed sensitivity to other abiotic factors such as UV radiation and heat. In yeast, some homologous recombination deficient types will be unable to repair damage from double strand breaks (DSB's) incurred by SSB's impeding the replication fork from proceeding (Lundin 2005). Once the replication machinery becomes corrupted and repair mechanisms cannot undo the damage to DNA, growth and development of the unicellular yeast will be affected negatively. Some of the affects attributed to MMS19 deletion in yeast include retarded growth at temperatures higher than 30°C, methionine auxotrophy (inability to synthesize this amino acid natively) and a thermo-labile defect in RNA Pol II transcription (Prakash 2000).

Role of MMS19 in cell

One of the original hypotheses for the function of MMS19 within a cell's metabolic activity included the idea that this protein played an indirect role in DNA repair. Although there are many different types of DNA repair mechanisms that exist within eukaryotes, one of the more complex repair pathways requires the use of RNA Pol II and its transcription factor TFIIH (Hatfield 2006). When MMS19 was first being described experimentally in yeast and mice, scientists could not find a direct correlation between the gene's function in DNA repair and growth. It was however clear those MMS19 mutants were deficient in a pathway of DNA repair called Nucleotide Excision Repair (NER). These mutants would be exposed to UV light with spectrums dominantly in the β-wavelength. This type of radiation is known to cause cyclobutane pyrimidine dimers (CPD's) in DNA which form lesions that become mutagenic to the cell. Assaying the quantity of these CPD's, scientists could detect that MMS19 mutants were incapable of removing these lesions adequately using NER (Lombaerts 1997). This supported the idea that MMS19 had a role in DNA repair in the specific NER pathway. What that role exactly was wouldn't be identified until several years later.

Researchers were also able to identify a transcriptional defect in MMS19 mutants. By studying the effects that temperature played on the yeast mutants, a thermo-labile defect in RNA Pol II was observed (Lauder 1996). After being exposed to 37°C during incubation, MMS19 mutants could no longer be transcriptionally active. Biochemical studies also revealed that purified MMS19 protein could not recover NER proficiency *in vitro* (Lauder 1996). This important finding indicated that MMS19 was not directly involved in the NER machinery, but instead acted as an upstream regulator of TFIIH which serves as a crucial transcription factor for

RNA Pol II. The physiological significance of MMS19 expands beyond its indirect role in NER and has serious implications for growth.

Some research has indicated the possibility that MMS19 plays some regulatory effect on the formation and maintenance of telomeres (Askree 2004). In this publication, MMS19 mutant yeast exhibited 50-150bp longer telomeres than the wild type. Although common understanding of telomere activity within the context of longevity and cancer prevention dictates shortening telomeres as being precursors to disease, longer telomeres may not be profitable to the cell. Cellular proliferation is energetically expensive and the ubiquitous extension of telomeres to prevent long term onset of disease is inefficient as natural selection usually occurs against cancer & other related diseases in the younger years of an organism. Instead a thrifty phenotype is hypothesized to be responsible for the shorter telomere needed for adequate survival within species.

Function of MMS19 as a scaffolding protein

Scaffolding proteins are characteristically molecules that have sequence motifs that encourage interaction with other proteins. MMS19 has 15 tandem repeats that have leucine rich motifs (LRM) (Lauder 1996). These LRM's are well documented to have a role in protein-protein interaction and are typical of DNA repair proteins (Peters 1996). The well conserved sequence homology across species for this gene also provides insight into the functional domains that are exhibited within taxa. From what can be inferred from alternative splicing that occurs within humans, there are three distinct domains for this protein (Hatfield 2006).

Functional domains of MMS19

Functional domains describe the different ways that protein molecules can interact with their environment inside the cell. Some of these domains may act as targets for the cell, allowing it to direct function in more than one way. Other domains within the protein sequence are useful for catalytic activity or in the case of a scaffolding protein, for building and attaching inorganics to amino acid residues. When certain domains are absent in the mRNA as a result of alternative splicing, the stability of the protein formed during translation may change. The C-terminus of the full length MMS19 sequence contains the four HEAT repeats associated with its binding to CIAO1 (Fe-S protein) and NARFL (Wietmarschen 2012). These proteins act as the Fe-S donor to the MMS19 protein during biosynthesis of this inorganic cofactor. The other two domains are A & B which coordinate the activity of the recipient protein XPD helicase. In turn XPD will then direct function of TFIIH holoenzyme in a transcriptional or NER preferential manner (Hatfield 2006). Domain A is cited as directing function of MMS19 when exposed (domain B missing) towards transcription, while an exposed domain B (domain A missing) directs function of TFIIH towards NER (Hatfield 2006). The method through which this occurs has been investigated separately and reveals that similar HEAT repeats are also found within the N-terminus of the MMS19 polypeptide (Wietmarschen 2012).

Biogenesis of Fe/S clusters

Inorganic cofactors are elements that play crucial roles in enzyme activity in all organisms. Without the necessary cofactors, tertiary structure of many proteins is not complete and cannot confer the function necessary for homeostasis. Some well-known cofactors that play important roles in biochemistry include Magnesium found within the porphyrin of chlorophyll pigments for photosynthesis and Iron within the heme found in hemoglobin necessary for red

blood cells. Fe-S clusters are usually tetrahedral polymetallic molecules held within proteins for structural and functional roles (Meyer 2008). They have an especially significant role in mitochondrial biochemistry, forming the essential platform for photosystem function in plants and oxidation-reduction reactions within the electron transport chain of mitochondria (Lill 2012). It is quite clear that these types of molecules are ubiquitous within the cell and necessary for many biochemical functions both rudimentary and highly specialized. Such is the significance of these types of biochemical interactions with proteins and the metals that an Iron-Sulfur world theory was formed by chemist Wächtershäuser (1997). In a new publication review the author here cites Wächtershäuser and describes the necessity of these inorganic cofactors to proper protein maturation within the mitochondria, cytosol and nucleus (Lill 2006).

The biogenesis of complex Fe-S clusters requires the modulation of chemistry between the mitochondria and the cytosol. Nuclear encoded genes shuttle to the mitochondria as proteins that aid in the biosynthesis of Fe-S necessary for so many of the cell's biochemical reactions (Rouault 2012). The basis for Fe-S clusters being incorporated into apoproteins relies on the mitochondrial output of these inorganic cofactors as well as a scaffolding complex using many proteins to attach the mature forms onto apoproteins. This entire biochemical system can be referred to as the cytosolic iron-sulfur cluster assembly (CIA) pathway (Luo 2012).

The entire biochemical synthesis of Fe-S clusters begins inside the mitochondria with a separate pathway termed ISC (iron-sulfur cluster). Maturation of these Fe-S molecules then continues by way of proteins such as NBP35, CFD1 and DRE2 within the cytosol (Van Wietmarschen 2012). The Fe-S cluster is then transferred onto a complex which includes proteins CIA1 and NAR1. The final step in forming this molecule includes several scaffolding proteins such as MMS19, MIP18, and ANT2 which act simultaneously by binding the Fe-S

donor to the target apoprotein (such as XPD helicase). The target protein is now complete and will be localized to the area in the cell where function dictates. In the case of DNA repair enzymes such as XPD helicase, it will shuttle to the nucleus where it will assemble with TFIIH core to begin nucleotide excision repair (Aguilar-Fuentes 2006).

Nucleotide Excision Repair (NER)

In the literature reviewed, Transcription Factor II H (TFIIH) is noted consistently as a necessary component for RNA Pol II function (Matsuno 2007). TFIIH was originally identified as playing a critical role in nucleotide excision repair in purification experiments that showed XPD mutations in yeast could be complemented with purified TFIIH enzyme (Wang 1994). This large enzyme interacts with many of the necessary DNA repair proteins created by the cell. The proteins involved in NER are numerous each with cross regulatory function to the DNA damage signaling response. NER can repair many different types of lesions including UV radiation induced photoproducts, cyclobutane pyrimidine dimers, bulky chemical adducts and free radical induced base lesions (Hatfield 2006). Without all the compliments of these proteins available to the NER machinery, the possibility of error or failure increases. Some components when mutated prove to be embryonic lethal to the organism while others don't present the effects of mutation until several weeks after. Ultimately there are key enzymes that when unavailable will produce a mutant phenotype which is well documented in yeast and animals including humans (Kamileri, 2012).

Transcription-coupled NER

The transcription of genes within an organism is dynamic to the environment and may be highly regulated or constitutive. RNA Pol II is one of the three transcriptional enzymes within

eukaryotes that catalyze the synthesis of pre-mRNA (Wilson 2013). At any moment during a cell's lifespan, RNA Pol II may encounter a damaged, missing, or altered base that prevents any further transcription of a gene. To combat this, the cell has developed a highly coordinated ensemble of repair proteins that locate the damaged base, excise it from the DNA and replace with a complimentary sequence from the anti-sense strand (Laat 1999). This method of targeting damaged genes that are being transcribed is beneficial as the detection signal is the halted RNA Pol II. Transcription coupled NER (TCR) is found to be conserved in yeast, animals and plants (Fidantsef 2012). Any defects within the NER machinery will result in transcription failure which in turn will create developmental defects within the organism (Kamileri 2012).

When RNA Pol II encounters a lesion or helical distortion that prevents further transcription of a gene, a CSB protein associated with UV-induced DNA damage response binds to the RNA Pol II and recruits the rest of the NER machinery (Kamileri 2012). TFIIH associates with the site of damage and ATP-dependent helicases like XPD/XPB begin to open the double strand to an area of around 25 base pairs in opposing directions. Several other protein factors associated with TFIIH play important roles in maintaining this open complex formation (Laat 1999). The excision step involves two endonucleases that remove the damaged site along with 2-8 nucleotides on the 3' incision and 15-24 nucleotides on the 5' incision (Laat 1999). The repair machinery at this point may disassociate from the damaged area along with the damaged olignonucleotide sequence recently removed. DNA replication now follows where DNA polymerases will copy the antisense strand and fill the missing gap with the correct bases.

Global genomic NER

Unlike transcription-coupled NER, global genomic NER (GG-NER) does not rely on a transcriptionally active DNA strand as a substrate (Kamileri 2012). Any exposed parts of the genome are available to the machinery. The way this is accomplished is by unique DNA damage-sensing proteins that identify lesions within DNA. A major player in the DNA damage signaling response is the XPC (Rad4) protein that identifies lesions across DNA (Laat 1999). This complex then recruits the repair machinery proteins that open and unwind the DNA for lesion repair. These damage response factors show a high affinity to UV induced damage such as cyclobutane pyrimidine dimers, so naturally a plant organism should have high constitutive levels of this gene expressed throughout the life cycle. This initial step of identifying DNA damage within the transcriptionally silent genome sometimes employs other DNA damage sensing agents such as UV-DDB (Laat 1999). After helical distortion from XPC binding to DNA damage sites, the rest of the core TFIIH repair machinery begins melting the double strand and repair begins. The rest of the steps are the same as those in TC-NER.

Maintenance of core TFIIH and CAK complexes

Fe-S clusters being necessary components of various enzyme activities have a unique association with mitochondria within a cell. Upon maturation of these inorganic cofactors, apoproteins arrive to the outer mitochondrial membrane where assembly proteins attach these inorganics to cysteinyl residues, forming a complete holoprotein (Van Wietmarschen 2012). After activation by MMS19, the target holoprotein will associate with TFIIH and begin its function in NER.

Mutations identified for genes associated with this process of maturation within the CIA machinery were labeled according to the disease presented by patients. Inability to repair DNA

lesions caused by ultraviolet radiation on skin may eventually lead to formation of melanomas. Individuals who have mutations in any of these proteins may show an increased susceptibility to oncogenesis. A particularly debilitating disease occurs where a mutation within a 5'->3' helicase diminishes NER function. Xeroderma pigmentosum (XPD) is a disease where the individual has no natural defense against the accumulation of DNA lesions. Ultimately the individual when exposed to ionizing radiation from the sun will develop extensive melanomas across all skin, eventually leading to death (Quiemado 2001).

XPD is the name given to the ATP-dependent helicase involved in unwinding DNA in a 5'->3' fashion for DNA repair and telomere maintenance (Lill 2012). Genes that share similar motifs and function include XPB and XPC. MMS19 is now implicated as being directly responsible for maintaining adequate amounts of these subunits within the cytosol (Kou 2008). MMS19 acts as a transitional scaffolding protein that allows Fe-S donors such as CIAO1 to transfer their Fe-S cluster to target apoproteins such as XPD/XPB (Van Wietmarschen 2012). These ATP-dependent helicases then associate to TFIIH core within the nucleus.

TFIIH is not only required for proper NER function, but also for transcription and cell cycle progression (Matsuno 2007). The directional function of TFIIH is hypothesized to be mediated by the presence or absence of its two major subunits. Core TFIIH consists of XPB helicase/ATPase and XPD helicase, p34, p44, p62 for DNA binding, and p52 which mediates binding between XPB and other elements (Matsuno 2007). The Cdk-activating kinases that comprise the rest of the holoenzyme are CDK7, Mat1 and Cyclin-H. *In vitro* studies suggest these cell cycle regulators are present in the holocomplex TFIIH and are sufficient for cell cycle progression (Fisher 2005).

If the necessary core TFIIH factors XPD/XPBdo not carry the right inorganic cofactor (Fe-S) their tertiary structure may not be adequate for assembly/binding to other parts of the holocomplex. Because MMS19 diminutive mutant is hypothesized to be incapable of seamless transfer of Fe-S clusters to necessary apoproteins (XPB/XPD), it would follow to observe several of the same phenotypes attributed to core TFIIH and CAK mutations. These pleiotropic phenotypes include G1/S cell cycle arrest (Matsuno, 2007), increased cell death (Hara-Nishimura, 2011), decreased cell proliferation, water deficit phenotype (Jiang, 2014), and premature vascular differentiation (Cools, 2011).

MMS19 gene expression in other organisms

Studies into the role of MMS19 have been conducted across other organisms besides *S. cerevisiae.* The benefit of sequencing and analyzing the composition of this gene across species allows for identification of conserved domains. The fact that DNA repair has remained an essential process for all organisms is credit to the biochemical sophistication of more than just one dedicated pathway. Other forms of DNA repair that can be found from single celled prokaryotes to single/multicellular eukaryotes include base excision repair (BE), homologous recombination (HR), mismatch repair, non-homologous end joining (NHEJ), and photoreactivation. MMS19 is so indispensable to proper NER function that it can be found nearly within all of eukaryote species as a homolog with conserved domains (Seroz 2000).

MMS19 function across species

Some of the species studied included other forms of yeast such as *Schizosaccharomyces pombe* and the well-studied *Arabidopsis thaliana.* Specifically in *Mus musculus* (house mouse) researchers were able to describe alternative transcripts of the MMS19 gene (Hatfield 2006).

Well conserved sequences of the gene were also described across species, primarily in the C-terminal domain of the polypeptide. These HEAT repeats are so called after a motif that establishes some relationship to scaffolding proteins through their solenoid domain (Quiemado 2001). Some of the other species that exhibit similar amino acid residues when compared to human and yeast cDNA for MMS19 are *Drosophila melanogaster*, *Caenorhabditis elegans*, and *Arabidopsis thaliana* (Seroz 2000). In some experiments it was illustrated that MMS19 yeast mutants could recover from their thermosensitive growth defect along with UV radiation sensitivity when human MMS19 cDNA was inserted under a GAL1 promoter (Quiemado 2001). This shows that the conserved domains still exhibit a large amount of their function even when divergence has occurred, leading to the theory that MMS19 is so necessary for CIA that is conserved well within all eukaryotic species (Stehling, 2012).

Cell cycle progression in plants

Because of the sessile nature of plant life, these organisms depend on growth phases and differentiation of cellular material into all of the different organs in a plant's natural history to be extremely well regulated. Like in all eukaryotic organisms, the G1, S, G2 and M phase retain their usual characteristics.

G2 phase and the DNA integrity checkpoint

Certain kinases have been identified in plants as being responsible for halting cell cycle progression into the mitotic phase. The negative regulator wee1 kinase originally described in yeast has been studied in *Arabidopsis* and proven to halt cell cycle progression (DeSchutter 2007). The action of this gene is to negatively phosphorylate cyclin-dependent kinases (CDK's) thereby preventing the onset of mitosis. The purpose of this is to assure the integrity of the

genome is complete and that no errors occurred during replication of DNA during S phase. Wee1 experiences its highest transcriptional patterns during S-phase and drops continuously as the cell enters G2-phase (Cook 2013). During a plant's cell cycle progression under normal growth conditions the replication errors and DNA damage accrued during development are identified via the ataxia-telangiectasia-mutated (ATM) and Rad-3 related (ATR) signaling pathways (DeSchutter 2007).

These pathways create a transient cell cycle arrest that allows for repair mechanisms to identify DNA damage and reverse it. Wee1 knock out plants do not show a different phenotype compared to wild type under normal growth conditions. However when exposed to replication stress factors, the absence of this gene affects normal cell cycle progression resulting in increased cell death and premature vascular differentiation in meristematic tissues (Cools 2011). Plants with induced wee1 expression undergo cell cycle arrest at G2 and do not continue on to mitosis (DeSchutter 2007). As DNA damage occurs constantly throughout the photoperiod, it would be expected for wee1 transcription to be upregulated in a DNA stressed mutant such as the MMS19 diminutive type. However because the MMS19 mutation hypothetically confers a nonfunctional XPD/XPB apoprotein, the ability to repair DNA damage itself would be compromised. This in turn would result in accumulation of DNA damage that when unrepaired signals to the cell through some proteolytic pathway that arrest or death must occur.

Autolysis, autophagy and vacuolar programmed cell death

Although plant cells undergo many of the same developmental cycles as those found in all eukaryotes, they are unique in the way that programmed cell death manifests itself. What is normally described as apoptosis within mammalian cells cannot be directly associated with the same phenomenon seen in plant cells (Reape 2008). In plants a rigid cell wall prevents the

formation of excess osmotic potential that would result in an animal's cell to burst. Instead, turgor pressure is created when osmotic potentials differ from the environment. Plants however do require a highly regulated system of cellular development that includes differentiation into other cell types along with apoptosis. Because plants do not have innate immunity in the same way that animals do, their primary line of defense against infection from parasites is to isolate the affected areas via necrosis (a form of plant apoptosis). One of the ways this is accomplished is through the signaling mechanism used in vacuolar programmed cell death where the large central vacuole plays a pivotal role in autolysing the entire cell (Hara-Nishimura 2011).

Growth effects and physiology under stress

Carica papaya is a tropical herbaceous plant that has robust growth in certain cultivars, resulting in a one year seed to fruit cycle (Ming, 2008). The need for rapid shoot and root development to compete for light sources is one of the possible selective pressures that allowed for evolution of this high growing tree. Because of these rapid developmental features, papaya can also be more susceptible to factors that limit growth such as salt stress, water stress, and genotoxic stress.

UV light sensitivity and drought stress in plants

Many plants have developed mechanisms to avoid excess transpiration of water during the diurnal cycle. Sometimes these molecular changes within the transcriptome result in a drought tolerant phenotype. The benefits that a plant experiences from this include decreased wilting of leaves and increased survival rate (Zhou 2013). Another defense that plants have developed through evolution is the resistance to damage from ultra-violet light. In some species growing in shaded areas promotes healthier development, but because plants are sessile

organisms they must also employ molecular mechanisms to resist UV damage. One mutation studied in *Arabidopsis* showed an increased tolerance to UV-B radiation that would normally kill wild type plants. This mutation increased the expression of chalcone synthase (CHS), the enzyme necessary for the first step in flavonoid biosynthesis (Bieza 2001). Flavonoids are plant secondary metabolites that are responsible for giving flowers their radiant colors (Liu, 2000). They have also been linked to absorption of UV-B radiation that is otherwise harmful to organisms through its damaging effects on DNA.

CYCH;1 is a cyclin that activates CDKD's which in turn play important roles in regulating cell cycle progression and transcription (Fisher, 2005). The silencing of this gene in *Arabidopsis* constructs have shown some of the downstream effects that occur in the absence of *CYCH;1*. When down regulated, a drought tolerant phenotype is observed in plants that are produced by the closing of stomatal openings within leaves. The response by stomatal guard cells is believed to occur due to accumulated levels of reactive oxygen species (ROS). It is also known that *CYCH;1* binds to and activates cyclin-dependent kinases that are responsible for phosphorylating the C-terminal domain of RNA polymerase II which is indispensable for proper transcription (Fisher 2005). Transcriptional changes for this gene may be tied to a drought tolerant phenotypic response, but have crossover linkage with TFIIH core factors as well (Matsuno 2007). MMS19 mutants do not have a direct link to transcriptionally changing the expression of downstream genes such as TFIIH, but are instead deficient in TFIIH activity (Lombaerts 1997).

Through these mutation studies different phenotypic effects caused by UV radiation and water deficit have been documented within *Arabidopsis*. Large efforts are placed on discovering the changes within the transcriptome of organisms when single gene mutations occur. MMS19

deficiency within the diminutive mutant may exhibit some of the same pleitropic phenotypes observed in yeast and animals.

Respiration and metabolism as affected by MMS19 mutation

Accumulation of starch grains within chloroplasts have been observed in plant research before, though for reasons other than genotoxic stress. β-amylase is a starch metabolizing enzyme that is well conserved across taxa within higher plants. The draft genome for *C. papaya* revealed that starch-associated genes are found in higher numbers within papaya in both the synthesizing and metabolizing areas (Ming, 2008). This chloroplast targeting enzyme is found within the leaves of plants and is responsible for breaking down starch reserves into maltose for transmobilization of sugars across tissues (Reinhold, 2011).

Some of the effects caused by excessive UV-B radiation on plants include changes to chloroplast structural integrity and decreased starch grains (Hollosy, 2002). Grana and stroma also appear to suffer damage and thylakoid membrane stability decreases. These observations were made on experiments conducted on *Lysimachia nummularia* which is a creeping perennial. Besides all of the deleterious effects caused by things such as UV-B radiation and water deficit, sugar signaling within plants may significantly alter the transcriptome of the organism at any given moment (Reinhold, 2011). Because of papaya's need for robust growth, cell expansion genes as well as starch-synthesizing genes are more abundant and necessary for storage of energy within leaves (Ming, 2008). All of this explains how papaya appears to have converged evolutionarily with other organisms in tree-like habitats.

The MMS19 mutation within *C. papaya* is not embryonically lethal, and doesn't present an obvious phenotype during germination. Because MMS19 deficiency is so heavily associated with transcriptional and DNA-repair deficiencies, a rapid growing perennial like papaya may be

more susceptible to downstream effects. A reduction to mRNA levels for starch synthesizing/catabolizing genes within papaya could possibly explain the increasing size of starch reserves within photosynthesizing chloroplasts. An alternative explanation to the altered physiological profile for papaya includes the possibility of an overall reduced energy profile for the MMS19 diminutive mutant.

CHAPTER III

MATERIALS AND METHODS

Sample collection

Two genotypes were chosen to describe the role of MMS19 mutation within *Carica papaya*. A MMS19 deficient mutant is included with homozygous recessive allele as a diminutive phenotype. A wild type of the same cultivar (SunUp) was used as the control with a homozygous dominant allele and normal growth phenotype. Tissues were collected from both the MMS19 mutant and wild type plants for electron microscope and light microscope analysis. Separate tissues were collected for total RNA extraction for molecular analysis. The samples were categorized by the following: wild – mature leaves, young leaves, flowers; mutant – mature leaves, young leaves, flowers.

Preparation of samples for TEM and light microscopy

Preparation of samples followed protocols dictated in Kuang et al. (2000). Specimens were collected from AgriLife field site for transmission electron microscope analysis. Leaves and flowers were fixed in 2.5% glutaraldehyde and 2% formaldehyde in 0.1 M phosphate buffer at pH 7.0 for two hours in room temperature. Samples were then washed with 0.1 M phosphate buffer to remove fixative. Post-fixation was done overnight with 1% osmium tetroxide. Tissues were processed in a serial dehydration using ethyl alcohol (EtOH). Dehydration began at 25%

for twenty minutes. The next change of ethyl alcohol continued at 50, 75, and 95 up to 100 % EtOH. Three dehydrations of 100% EtOH were done for each sample. Infiltration through gradients using LR white resin (London Resin Co LTD) followed at room temperature. Samples were placed on an Infiltron tissue rotator to increase infiltration of resin. Three changes of pure resin at an hour each were done for each sample. Tissues were transferred into embedding capsules with fresh resin and then cured in a vacuum oven for 24 hours at 68°C.

Resin blocks were trimmed and prepared for microtomy using a double sided razor. A Leica Ultracut R microtome (Leica Microsystems) was used to section at 70 nm thickness using a MicroStar diamond knife (Micro Star Technologies). Sections were mounted on 300 square mesh copper grids, stained in 5 % uranyl acetate for 15 minutes followed by a lead citrate stain for 5 minutes. Grids were dried completely and observed under the LEO 900 TEM at 50 kV (Zeiss). Images were visualized using a custom ADM digital mounted camera.

For visualizing under light microscope, semi-thin sections were taken using a glass knife prepared by Leica EMKMR2 glass cutter (Leica Microsystems). The sizes of sections were cut at 350 nm thickness using the Leica Ultracut R microtome. Whole sections were mounted on a drop of deionized water on superfrost plus slides. The sections were stained using 1% TBO. A coverslip was added for each slide prepared and dried out overnight. Leaves were visualized using an Olympus BX40 fluorescent microscope with an Olympus DP12 digital camera (Olympus Corporation).

Preparation of samples for SEM

Primary fixation of samples collected from AgriLife field occurred with a mixture of 2.5% glutaraldehyde and 2% formaldehyde in 0.1M phosphate buffer at pH 7.0 for two hours at room temperature. A 20 minute wash with 0.1M phosphate removed fixative and was done twice

for each sample. No post-fixation treatments were made on samples. Dehydration began with 25% EtOH and continued to 100% at twenty minutes each step. Three changes of 100% EtOH were done for each sample. Tissues were removed from vials and placed in a Tousimis specimen holder submerged in 100% EtOH. The specimen holder was then placed within the chamber of a Samdri-780B critical point dryer where final dehydration was completed in liquid CO_2. Tissues were then mounted on metal stubs and etched in a DESK II Denton vacuum. Samples were sputter coated with 10nm gold particles and viewed in an EVO LS10 scanning electron microscope (Zeiss). The Smart SEM user interface captured images of leaf surface and stomatal openings.

BLAST sequence identification of NER and reference gene orthologs

After reviewing the literature for possible downstream regulated genes linked to MMS19, several genes of interest were chosen as candidates for mRNA quantitative analysis. Qualifications for genes included association with TFIIH holocomplex, cell cycle controls, and starch metabolism. To identify putative orthologs for genes within *Carica papaya*, *Arabidopsis thaliana* candidate genes were located through The Arabidopsis Information Resource database (TAIR). The representative gene model was selected and the nucleotide sequence acquired. A link to GenBank revealed the accession sequence for each gene. The genomic data file was chosen and downloaeded with 1kbp's on both ends for "wiggle room" to identify mRNA. Using a BLASTn query on NCBI, gene sequences were selected based on hits and homology. mRNA for *C. papaya* was selected from highest probability candidates through Phytozome.net 10.2 genome search.

Primers were designed for amplification of these genes based on short amplicon length (small fragments between 100-250 bp) using Primer3. Primer design was checked for GC%

content and any hairpin formation using NetPrimer. The total number of genes identified as putative orthologs within *C. papaya's* genome include eight genes of interest and three house-keeping genes (See Table).

House-keeping reference genes	Gene	Sequence	TM
>Cp_75	EIF 50-69_F	TGAATGTCAGAGGCAGGCAA	59
>Cp_76	EIF 180-199_R	GCTTCTTTGCATCCTCGTGA	58
>Cp_77	EIF 38-57_F	GCGGAGTTGTCGTGAATGTC	58
>Cp_78	EIF 122-141_R	CTTCCACTGCTTCCCAATGC	60
>Cp_79	GAPDH 535-554_F	ACCGTCCATGCCATTACTGC	60
>Cp_80	GAPDH 692-712_R	GAACACGGAAAGCCATGCC	60
>Cp_81	GAPDH 687-706_F	ATTGACTGGCATGGCTTTCC	59
>Cp_82	GAPDH 780-800_R	GCCTCCTTGATAGCAGCTTTG	59
>Cp_83	EF1 677-696_F	CCAAGAGGCCGTCAGACAAG	60
>Cp_84	EF1 869-888_R	AACATTGTCGCCGGGAAGAG	62
>Cp_85	EF1 1044-1063_F	GCTCGACTGCCACACATCTC	58
>Cp_86	EF1 1173-1192_R	TGGGCTTGGTTGGAATCATC	60
Genes of interest	Gene	Sequence	TM
>Cp_01	CYCH1 708-727 F	TCTGAGCAGCATCGTCTCTT	58
>Cp_02	CYCH1 889-908 R	CTCCCGTTTCTTACTGCAGC	58
>Cp_03	CYCH1 387-406 F	GGAGGAGCTTGGAAAAGGGA	59
>Cp_04	CYCH1 613-632 R	AACAAAAGTGGCGCATCAGT	58
>Cp_11	XPC 1575-1594 F	GAGCTCTTTTGTTGCCACCA	58
>Cp_12	XPC 1756-1775 R	CGAGGGTAGACTGGATGACC	58
>Cp_17	XPC 1656-1675 F	CCAGCAGGCATACAAGAACC	58
>Cp_18	XPC 1800-1819 R	CCCGCAGCCATCTTTCTTTT	59
>Cp_21	XPD 904-924 F	ACACCTGGCTAGCAAATCCT	59
>Cp_22	XPD 1064-1083 R	GAGAGACGCAACAAAGCCAA	59
>Cp_23	XPD 824-843 F	CCACTGATGCGGGAAGATTG	58

>Cp_24	XPD 1019-1038 R	AGTTTCAAGACGCCCTCTCA	58
>Cp_31	SAM 189-208 F	GGCTGACGTCGACTATGAGA	58
>Cp_32	SAM 369-388 R	ACATATGGCCTTGGTCACCA	59
>Cp_33	SAM 369-388 F	TGGTGACCAAGGCCATATGT	59
>Cp_34	SAM 596-615 R	TGTGACTGTCTCATCGTGCT	59
>Cp_41	CT 531-550 F	TCTCAAGGTGCAGGCTGTTA	58
>Cp_42	CT 742-761 R	GCACGCATGAAGTCAGCATA	58
>Cp_45	CT 1439-1458 F	TGCCTAGGTACGACGAATCC	58
>Cp_46	CT 1654-1673 R	ACAAAATGCTCAGCTTCCCG	59
>Cp_51	XPB 1141-1160 F	GGTGGTAAACGGTCAGAGGA	59
>Cp_52	XPB 1274-1293 R	AAGCCCCAATTTGCAGTGAG	59
>Cp_55	XPB 2028-2047 F	CTACCACAGTCAGGAGGAGC	59
>Cp_56	XPB 2226-2245 R	TCACATTGCCTTGCCCTAGA	59
>Cp_61	CDKD 911-930 F	CTAAGCTCCCTAGACCTGCC	58
>Cp_62	CDKD 1072-1091 R	GGCACCTGTTCATTACCACG	59
>Cp_63	CDKD 892-911 F	CCTCTACCCACAGATCCAGC	59
>Cp_64	CDKD 1029-1048 R	GCACATTAACAGCAGACCCC	59
>Cp_71	WEE1 726-245 F	TGAGCAAATTGGTGTTGGCA	58
>Cp_72	WEE1 872-891 R	TTCATGAGACCCTAGTGCCG	59
>Cp_73	WEE1 996-1015 F	CGAGGGAGAAGTGCTGGTAG	59
>Cp_74	WEE1 1152-1171 R	ATGTGTGGCCAGGAAGAAGT	59

Table 1 – Primers designed for house-keeping genes and NER related orthologs for *Carica papaya*. Primers used for qRT-PCR are highlighted in green.

Fluorescence confocal microscopy

Tissues selected for visualization under laser scanning confocal microscopy were leaves from developing plants for both the MMS19 diminutive and wild type. Samples were excised from plant and fixed in 2.5% glutaraldehyde and 2% formaldehyde in 0.1 M phosphate buffer at pH 7.0 for two hours in room temperature. A 0.1 M buffer wash rinsed out fixative and serial ethyl alcohol dehydration began at 25% EtOH through 50%, 75%, 95% and 100%. After

reaching 100% EtOH during dehydration, tert-Butyl alcohol was used as transitional reagent to continue dehydration. For this transition, samples were placed in vials and kept at 30°C to maintain liquid phase of tert-Butyl alcohol. Three pure changes of tert-Butyl alcohol were done for each sample and continued with infiltration using heated paraffin at 56°C. Tissues were then mounted on steel paraffin blocks and cooled to solidify. Samples were trimmed and prepared for sectioning on a Leica RM 2135 microtome. Sections of 5 µm were taken and placed on a warm water bath then mounted on superfrost slides. Staining of slides was done using a Hoechst-33342 16 µg/mL concentration to identify viable cells by intact nuclear fluorescence. Staining lasted for twenty minutes and slides were then washed with PBS buffer and then treated with xylene to remove paraffin. Glass cover slips were mounted for each slide and visualized on a FluoView FV10i confocal laser scanning microscope.

Samples were analyzed using ImageJ and quantified for fluorescence signal. The threshold for fluorescence signal was adjusted to account for nuclear content specifically. Pixels were measured and exported as an excel file. Total signal was divided by the average surface area to calculate for approximate cell number. A two sample t-test was used to calculate for statistical significance. A probability level of 0.05% was used with 4 degrees of freedom.

Total RNA extraction for alternative splice detection

For molecular analysis of gene expression profiles for MMS19, tissues were harvested from AgriLife field site circa spring 2013. Mature leaves, young leaves and fresh flowers were excised from the plant from both MMS19 diminutive and wild type and placed in ice immediately. Samples were then placed into a ceramic mortar and immersed in liquid nitrogen, crushed and pulverized into a fine powder within the lab.

RNA extraction was conducted using the IBI Scientific Total RNA Mini Kit (Plant).

Real-time quantitation of NER related genes

All of the downstream genes identified for the MMS19 mutation were initially tested using PCR to confirm proper binding and amplification of products. Primers designed were tested for efficiency and quality of product.

Labeling and dilution of oligos primers began with 100µm original concentration to a final concentration of 2µm using milli q water. Primers were labeled separately for forward and reverse amplification. cDNA was tested using reference gene CNH3 primer set to measure quality of material for gene amplification analysis. With newly synthesized cDNA and older previously used cDNA CNH3 was amplified using a maser mix of enzyme and both primers. Improper melting temperatures (TM) and cDNA synthesized were identified as problems affecting amplification of gene products. New RNA extraction was done to reduce error and assure quality products for real time quantification. Tissues selected for RNA extraction were young leaves for both the MMS19 diminutive and wild types. This was chosen to select for a sample with a larger metabolic profile so as to provide more accurate results. DNAse treatment was done for both RNA samples to remove any possible genomic contamination. First-strand synthesis was conducted using reverse transcriptase to create cDNA. Reference genes selected for this experiment were chosen from Genbank for their quality as housekeeping genes. GAPDH, EIF4, and EF-1 were chosen and homologs found within the papaya genome. Primers were designed to amplify small fragments (<200bp) for qRT-PCR.

Care was taken to design an infallible qPCR worksheet and platform for results to be optimal. Below is the format of reagents, buffers and temperatures used for qRT-PCR. All 11 total reactions include 8 genes of interest and 3 reference genes. All reactions were done in triplicate as per normal qRT-PCR protocols dictate. For each of the 11 genes studied, one –RT

sample was included with primers A & B (forward and reverse), SYBR Green master mix for quantitation, and dH_2O included with cDNA that had no reverse transcriptase added during synthesis. This was done as a negative control to assure the researcher that amplification was restricted to sites with cDNA synthesized using reverse transcriptase.

Column1	Column2	Column3	Column4	Column5
WCp3 & Cp4 #1	WCp17 & Cp18 #1	WCp21 & Cp22 #1	WCp31 & Cp32 #1	WCp45 & Cp46 #1
WCp3 & Cp4 #2	WCp17 & Cp18 #2	WCp21 & Cp22 #2	WCp31 & Cp32 #2	WCp45 & Cp46 #2
WCp3 & Cp4 #3	WCp17 & Cp18 #3	WCp21 & Cp22 #3	WCp31 & Cp32 #3	WCp45 & Cp46 #3
WCp3 & Cp4 (-RT)	WCp17 & Cp18 (-RT)	WCp21 & Cp22 (-RT)	WCp31 & Cp32 (-RT)	WCp45 & Cp46 (-RT)
MCp3 & Cp4 #1	MCp17 & Cp18 #1	MCp21 & Cp22 #1	MCp31 & Cp32 #1	MCp45 & Cp46 #1
MCp3 & Cp4 #2	MCp17 & Cp18 #2	MCp21 & Cp22 #2	MCp31 & Cp32 #2	MCp45 & Cp46 #2
MCp3 & Cp4 #3	MCp17 & Cp18 #3	MCp21 & Cp22 #3	MCp31 & Cp32 #3	MCp45 & Cp46 #3
MCp3 & Cp4 (-RT)	MCp17 & Cp18 (-RT)	MCp21 & Cp22 (-RT)	MCp31 & Cp32 (-RT)	MCp45 & Cp46 (-RT)

Column6	Column7	Column8	Column9	Column10
WCp55 & Cp56 #1	WCp61 & Cp62 #1	WCp71 & Cp72 #1	WCp75 & Cp76 #1	WCp79 & Cp80 #1
WCp55 & Cp56 #2	WCp61 & Cp62 #2	WCp71 & Cp72 #2	WCp75 & Cp76 #2	WCp79 & Cp80 #2
WCp55 & Cp56 #3	WCp61 & Cp62 #3	WCp71 & Cp72 #3	WCp75 & Cp76 #3	WCp79 & Cp80 #3
WCp55 & Cp56 (-RT)	WCp61 & Cp62 (-RT)	WCp71 & Cp72 (-RT)	WCp75 & Cp76 (-RT)	WCp79 & Cp80 (-RT)
MCp55 & Cp56 #1	MCp61 & Cp62 #1	MCp71 & Cp72 #1	MCp75 & Cp76 #1	MCp79 & Cp80 #1
MCp55 & Cp56 #2	MCp61 & Cp62 #2	MCp71 & Cp72 #2	MCp75 & Cp76 #2	MCp79 & Cp80 #2
MCp55 & Cp56 #3	MCp61 & Cp62 #3	MCp71 & Cp72 #3	MCp75 & Cp76 #3	MCp79 & Cp80 #3
MCp55 & Cp56 (-RT)	MCp61 & Cp62 (-RT)	MCp71 & Cp72 (-RT)	MCp75 & Cp76 (-RT)	MCp79 & Cp80 (-RT)

Table 2 – qRT-PCR spreadsheet used to prepare 96 well plate for mRNA quantitation

The method used to calculate quantities of reagents used were for a single triplicate for 'X' gene of interest were n(reactions) + 1 to accommodate for volume loss during prep. 10µL of SYBR Green, 1µL of Primer A, 1µL of Primer B, 7µL of dH_2O, and 1µL of cDNA were used for each reaction. Master mixes were made for each primer set and cDNA added separately for tissues MMS19 diminutive mutant and wild type. All reactions were added to a MicroAmp® Optical 96 Well Reaction Plate. The plate was placed in a Labnet MPS 1000 Miniplate spinner to quick spin solutions to the bottom of the plate for optimum performance. A MicroAmp® Optical adhesive film was placed on the plate and sealed.

Program chosen for amplification of products followed Applied Biosystems recommendations. Times and temperatures for cDNA quantitation followed 2 minute HOLD at 50°C for activation, then a 10 minute HOLD at 95°C for DNA Pol activation, followed by a 40 cycle step of 15 seconds for melting at 95°C and 1 minute for annealing/extension at 60°C (T.M.) for the entire reaction. Storage temperature of 4°C kept reactions steady until recovery by the researcher. Program data was saved on USB and transferred to a computer for analysis using LineReg PCR (2012.x). An excel spreadsheet was exported for mathematical analysis. For quantitation of mRNA levels using reference genes for both MMS19 diminutive mutant and wild type, all genes of interest were analyzed using the Pfaffl (Pfaffl, 2001) equation published for relative quantitation. Ct's (critical thresholds) were used from reactions that had consistent amplification curves and few aberrations. Relative levels of mRNA were then graphed for each gene as a ratio to the wild type.

All setup and mixing of PCR samples took place in an isolated area under minimal light conditions and with positive-displacement pipette tips. A gel electrophoresis was conducted on

all qRT-PCR reactions to verify conformity and proper band formation so as to eliminate genomic or -RT contamination.

Immunocytochemical labeling

A PBS buffer solution was prepared in lab with a 1X concentration using 8g of NaCl, 0.2g of KCl, 1.44g of Na_2HPO_4, and 0.24g of KH_2PO_4. pH was measured and adjusted to 7.0. A desired 10mM PBS solution with 0.1% BSA (bovine-serum albumin) was prepared by adding 0.1g of BSA into 100ml of PBS and kept in 4°C for 1 hour.

Grids with 70 nm thickness sections were transferred onto drops of PBS for incubation to inactivate residual aldehyde groups. Primary antibody solution was prepared with a working concentration of 10 µl in 200 µl of PBS (1/20 dilution). A drop of the primary antibody was placed on paraffin paper and grids were transferred onto drops. Conjugation lasted for one hour. An incubation buffer wash was conducted on each grid six times at two minutes each wash. Gold conjugate reagent was prepared with a working concentration of 10 µl in 200 µl of PBS (1/20 dilution). Grids were transferred onto the drop of gold reagent for thirty minutes. Grids were then washed on drops of incubation buffer three times at two minutes each wash. A purely PBS wash was conducted three times at two minutes each wash. Grids were then fixed in 1% glutaraldehyde for 5 minutes. A distilled water wash was conducted four times at one minute each to remove any residual fixative. The estimated size of each nanoparticle of gold measured at 28.8 nm in diameter.

CHAPTER IV

RESULTS

Characterization of phenotype using microscopic technique

Light microscopy images

Observation of leaves under light microscopy showed some interesting differences between the wild type and MMS19 mutant leaf tissue. Size of cells within the MMS19 mutant appeared to be different along with the amount of differentiation and proliferation (not measured). Young leaves that were excised from developing stems of the plant apex showed some features of developmental delay. In Figure 1 the mutant leaf has fewer cells developed in the palisade and spongy layers. The epidermal layers of both leaves are present and appear differentiated at this developmental stage. Chloroplasts within the wild type are distributed evenly around the palisade parenchyma cells. The layer between the upper epidermis and palisade parenchyma within the mutant appears clear with chloroplasts clumping in the lower area of the cells (Fig. 1).

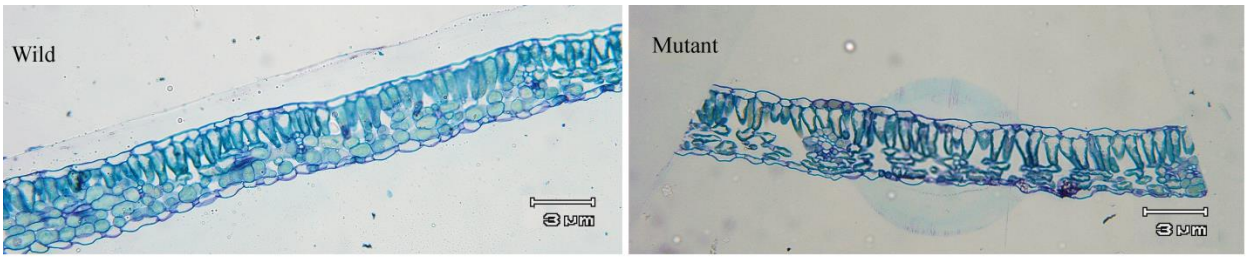

Figure 1 – Light microscope images of young papaya leaves stained with 1% TBO.

Magnification = 100x

When compared in overall size, the width of the MMS19 mutant leaf was smaller than that of the wild type, indicating that growth is different for the mutant. Cellular proliferation within the MMS19 mutant was also noted within the images captured.

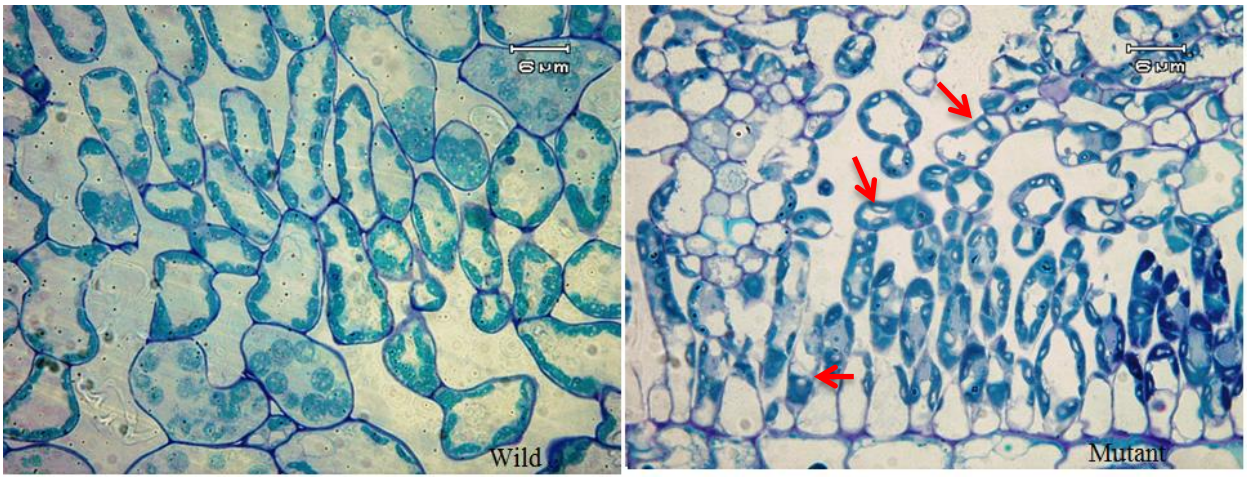

Figure 2 – Light microscopy images of mature papaya leaves stained with 1% TBO. Magnification = 1000x.

Another evident feature of the MMS19 mutant is an increased amount of starch grains found within the chloroplast (see Figure 2). These white grains are visible inside the stained chloroplast and are abundant across each cell (see arrows). When compared to the wild type, the amount of visible starch grains is nowhere near the same quantity as the MMS19 mutant.

As had been proposed by Dr. Yu before, some wrinkling of the cell wall within the mutant had been a feature associated with the MMS19 deficiency. In order to confirm this observation, more samples of mature leaves were processed and imaged under light microscope. The new images revealed some startling physiological occurrences within MMS19 mutant. What appears to be wrinkling of the upper epidermis is in fact apoptotic death of cells (See Figure 3). Cells immediately below the upper epidermis of the MMS19 mutant leaf also appear to be clumping their chloroplasts downward, away from the surface of the leaf. Some of these cells also show no signs of viable nuclear or vacuolar activity, indicating apoptotic death. Quantitation of cellular size and number revealed that indeed the MMS19 mutant showed fewer cells per surface area than the wild type (Figure 3A).

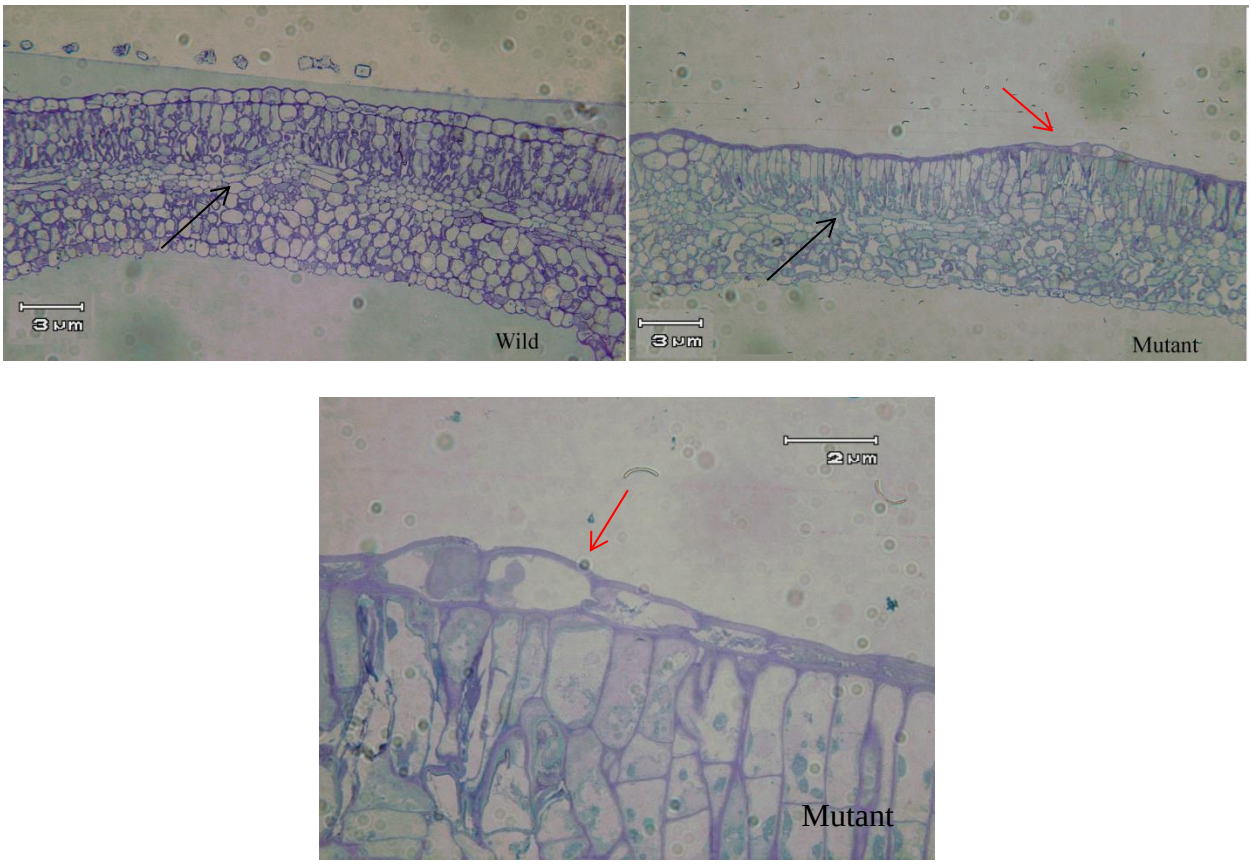

Figure 3 – Light microscopy images of mature papaya leaves stained with 1% TBO.

Magnification = 200x (top), 600x (bottom).

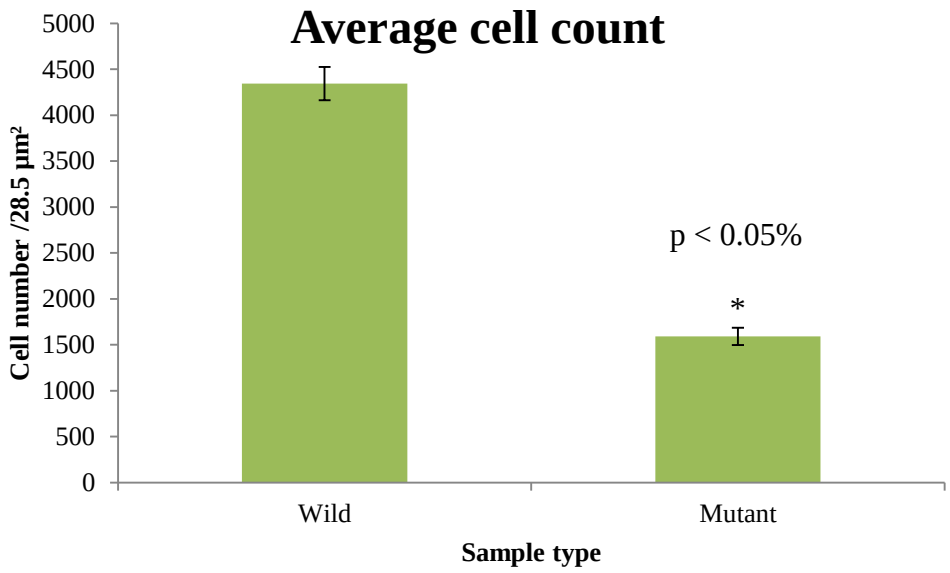

Figure 3A – Cell count of mature papaya leaves from light microscopy image. Wild type = 4,343 cells and mutant = 1,592 cells.

Another feature observed within the MMS19 mutant when compared to the wild type is the lack of consistent vascular differentiation. As can be clearly seen across the separation of the palisade and spongy mesophyll, a vascular bundle runs across the layers of tissue providing the necessary access to xylem and phloem for all cells. In the MMS19 mutant, there are disjunctions between xylem cells following the vascular bundle across the leaf tissue. The vascular cells are identified by the ring-like structures stained blue within otherwise empty cells (Figure 3 black arrows).

Flowers appeared to be developmentally retarded in the MMS19 mutant, as size was smaller overall. Fruit development within the MMS19 mutant did occur albeit at a slower growth rate than the wild type. It can be assumed that successful pollination of the mutant flowers occurred, but the extent to which the MMS19 mutant itself produced viable pollen would require more extensive measurement. Pollen viability was measured by looking internally at the anthers

of blooming flowers. Developmentally mature anthers would produce tricolpate pollen grains with folly formed endospore, exospore and perispore layers. The internal material appears dark from TBO staining under the microscope and can be inferred as viable if the pollen grain is morphologically round. Images of the anthers of the wild type control reveal stable spore content along with fully formed endospore and exospore. In drastic comparison, the MMS19 mutant anther shows a high degree of pollen non-viability. Many of the potential pollen grains appear to have undergone developmental arrest and show no stable genetic content inside (See Figure 4).

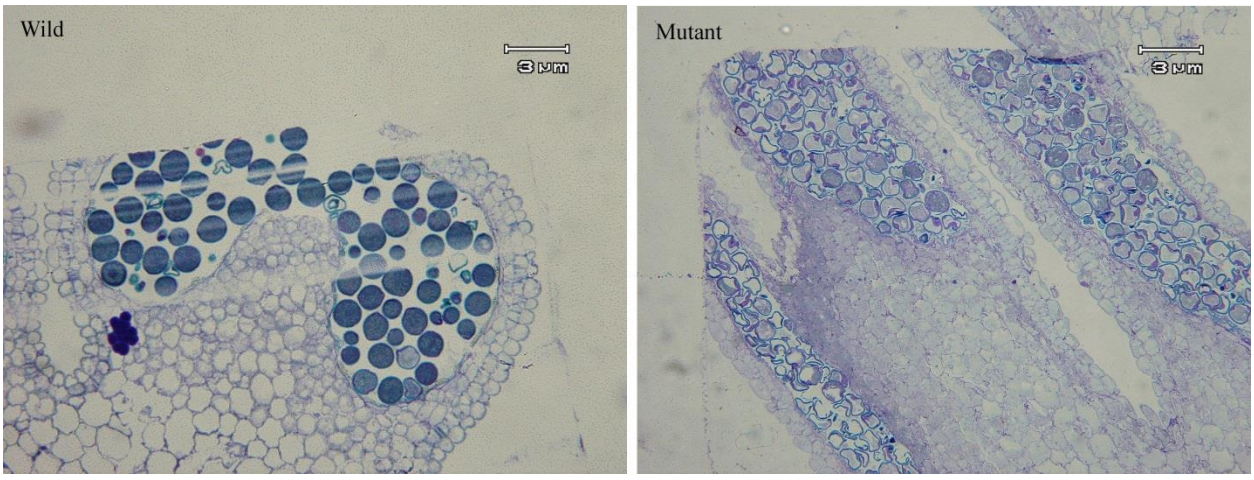

Figure 4 – Light microscope image of papaya anthers stained with 1% TBO. Magnification = 200x

As can be seen in the wild type, a viable pollen grain contains a well-defined spherical shape along with a darkly stained cytoplasmic content. The MMS19 mutant however shows many pollen grains in a developmentally arrested state, with limited content inside. These pollen grain aborts can be considered non-viable and detrimental to the plant's breeding capability.

Transmission electron microscopy images

Initial observation of plant leaves under high magnification EM showed some startling differences between the wild type and *MMS19* mutant. When compared to the wild type cells, the mutant large central vacuole showed high amounts of autolytic activity as can be seen in Figure 5.

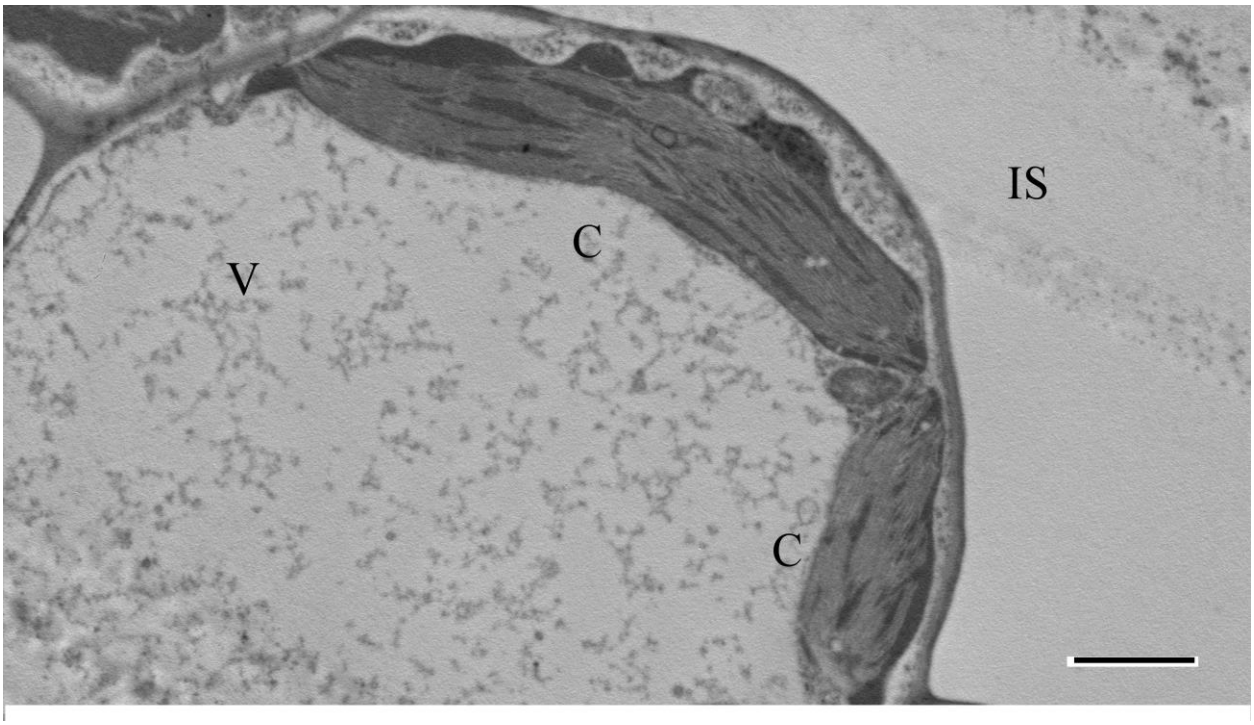

Figure 5 – TEM micrograph of wild type leaf cell. V = vacuole, C = chloroplast, IS = intercellular space. Bar = 2µm

The wild type cells show a large central vacuole with no autolytic activity and large chloroplasts within the periphery. Intercellular space is devoid of large fragments or debris. Chloroplasts show well-defined grana stacks and thylakoid membranes.

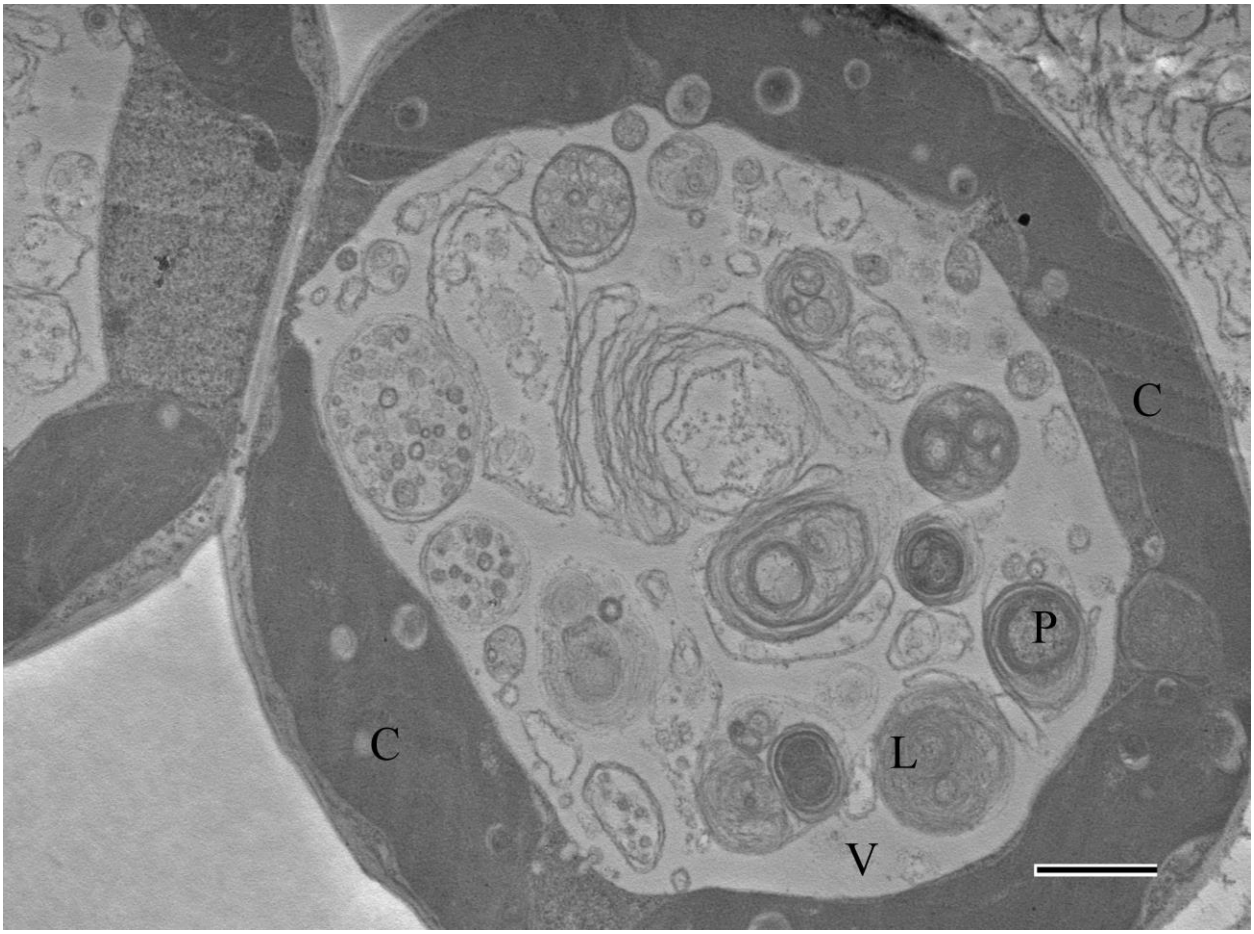

Figure 6 – TEM micrograph of MMS19 mutant leaf cell. L = lysosome, P = perixosome, C = chloroplast. Bar = 2 µm.

A large number of contrasts are visible within the MMS19 mutant leaf cell. Many of the autolytic activities occurring within the cell are compartmentalized to the central vacuole. These include peroxisomes digesting cellular material, lysosomes degrading plastids and bulk cytoplasm (Figure 6). Chloroplasts are visible although their grana and thylakoid membranes are not well defined. Starch grains and oil droplets appear to be developing within the chloroplasts. The overall shape of the cell is also constricted, as if the vacuole is exerting turgor pressure on the plasma membrane. These are some of the features associated with vacuolar programmed cell death.

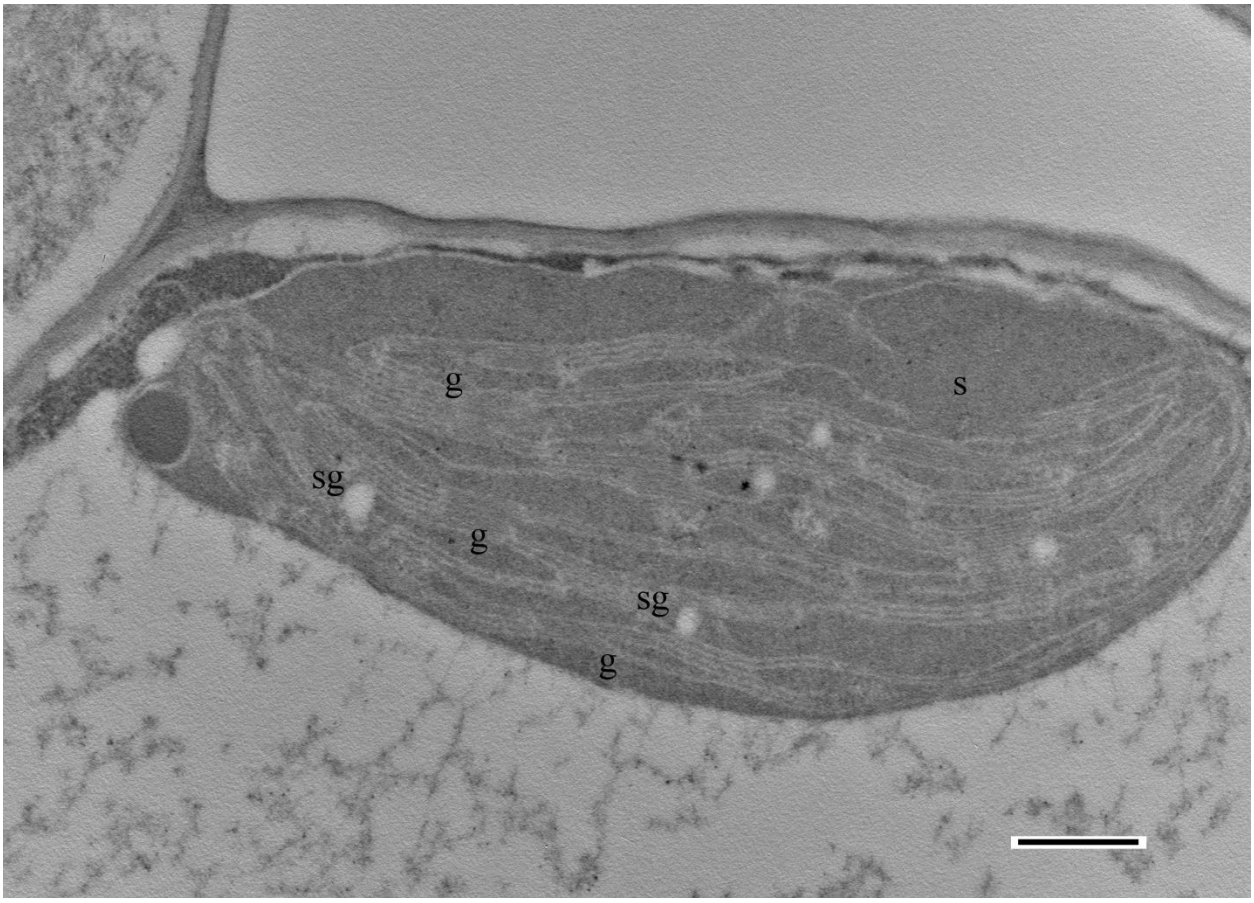

Figure 7 – TEM micrograph of wild type chloroplast. sg = starch grain, g = grana, s = stroma. Bar = 500 nm

In the wild type (Figure 7), chloroplasts show developing starch grains measuring less than 100 nm in diameter. The thylakoid membranes of the chloroplast are well defined and the overall shape of the organelle appears healthy.

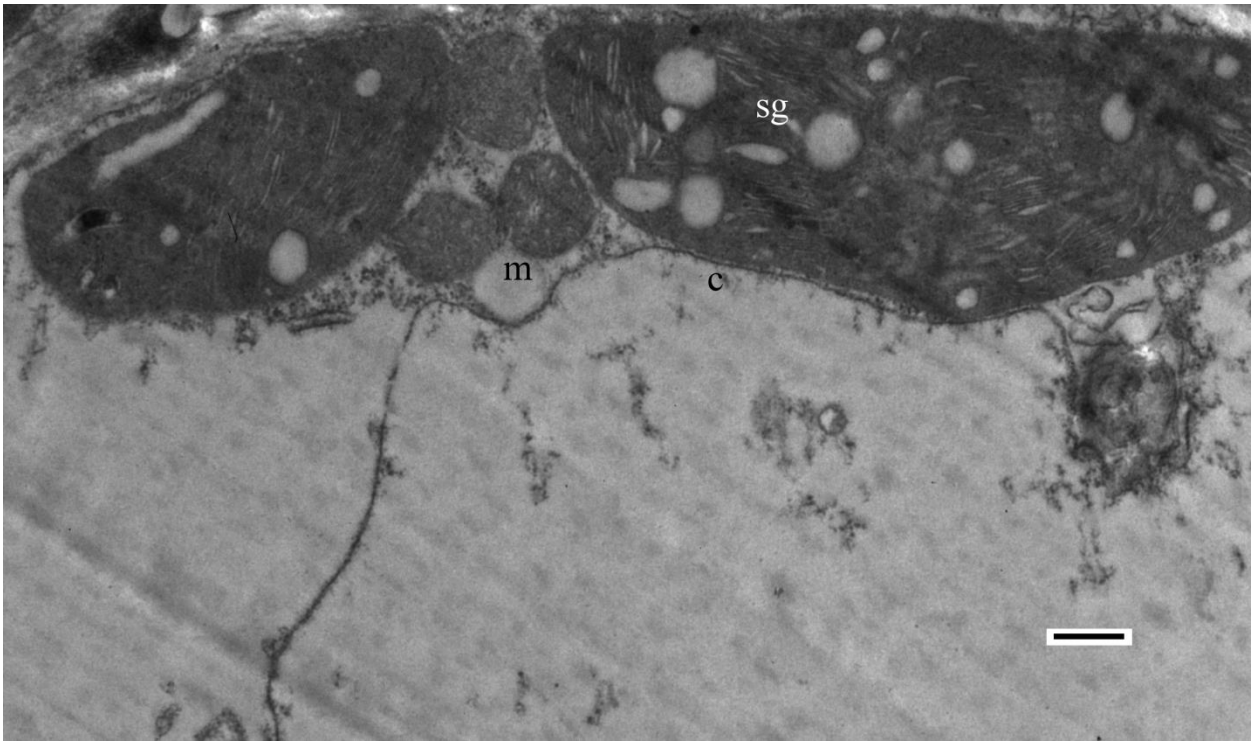

Figure 8 – TEM micrograph of MMS19 mutant chloroplasts. m = mitochondria, c = chloroplast, sg = starch grain. Bar = 500 nm

What is notably different about the MMS19 mutant cells are their high levels of starch grain accumulation within the chloroplasts (Figure 8). The organelle itself also appears to have less reticulated network of thylakoid membranes. Photosynthetic capability of the MMS19 mutant may be indirectly affected by what could be physiological changes occurring across tissues.

Another feature of autophagic death to cells is the consumption of organelles and fragments into the vacuole for degradation. In this figure of the mutant cell, a mitochondria can be seen undergoing endocytosis (Figure 9).

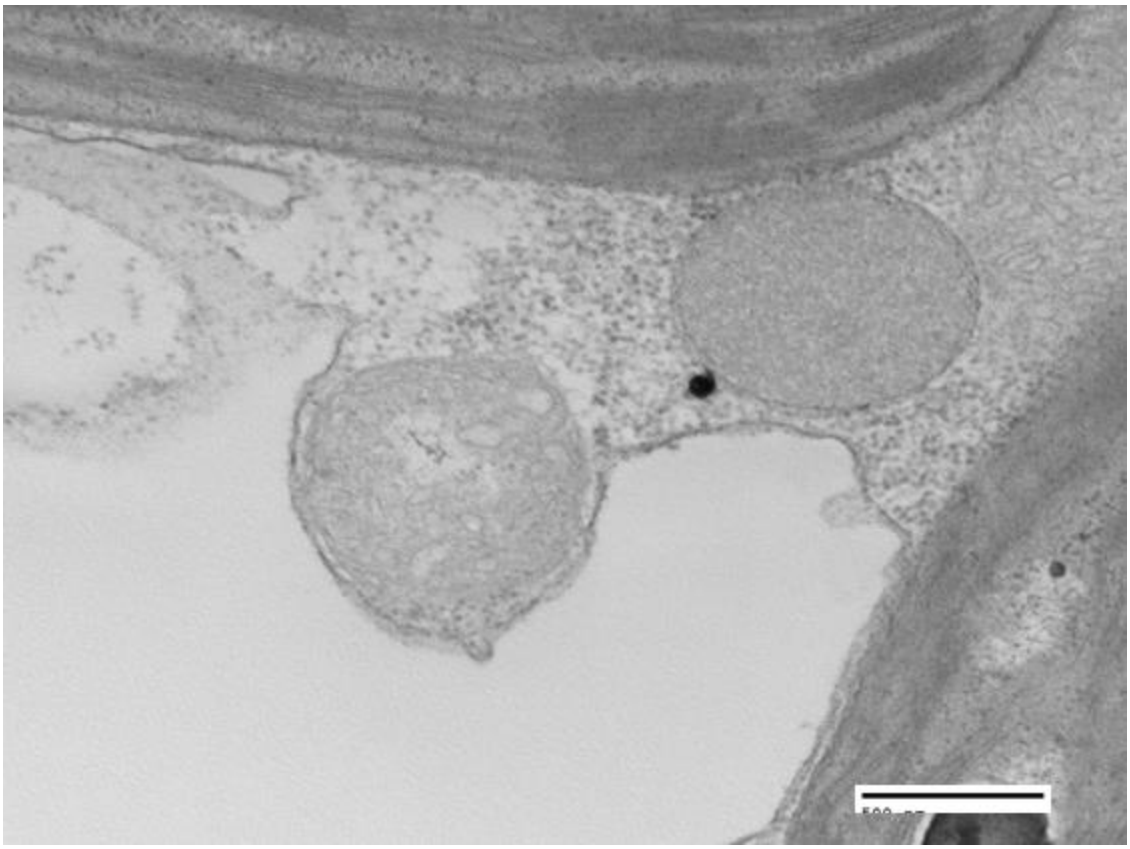

Figure 9 – TEM micrograph of MMS19 mutant with mitochondria undergoing vacuolar endocytosis. Bar = 500 nm

Other micrographs of the MMS19 mutant showed what appeared to be apoptosis at first and were later identified as vacuolar programmed cell death (VPD). These images show how nuclear instability and cell cycle arrest result in premature death of the cell.

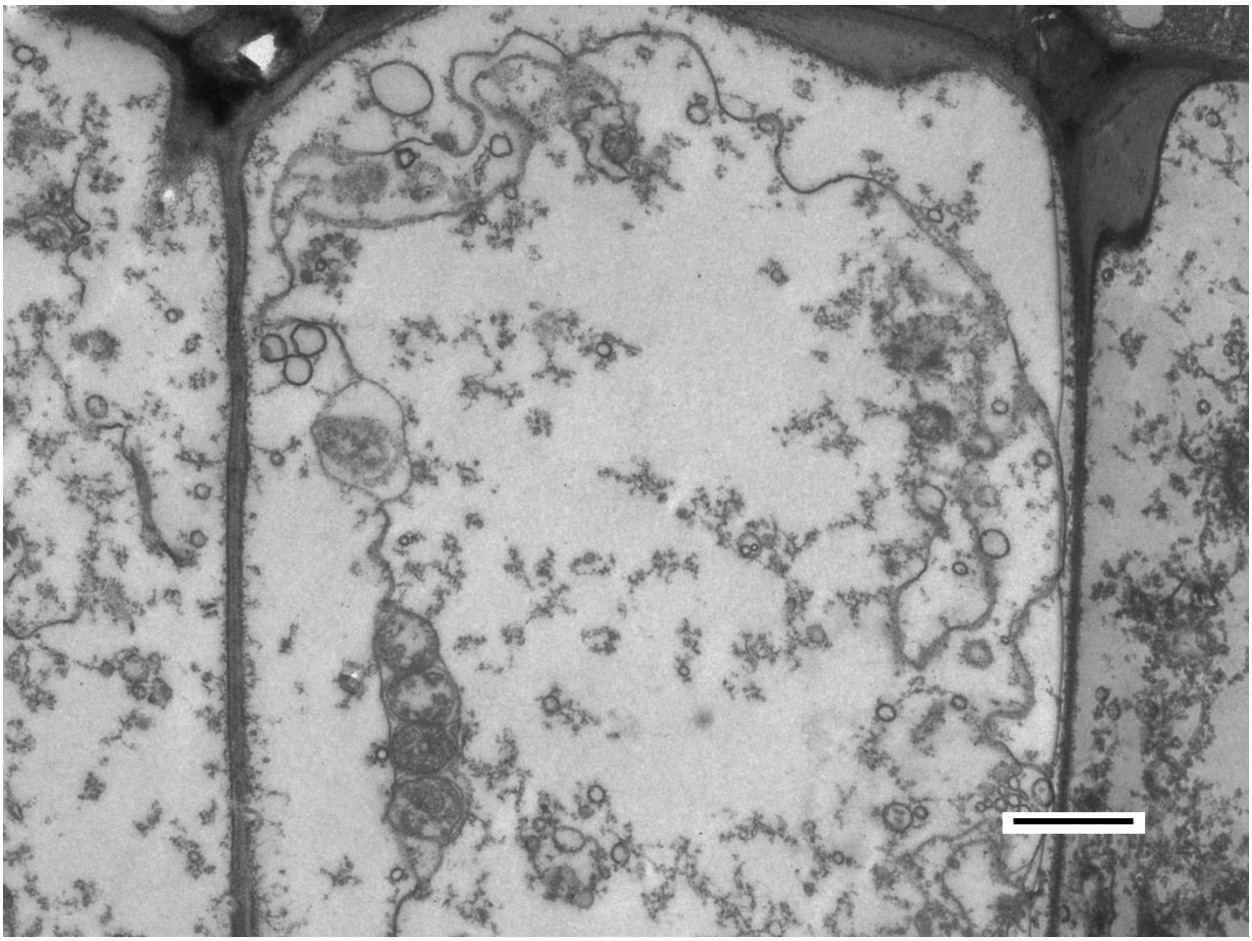

Figure 10 – TEM micrograph of MMS19 mutant anther cell undergoing vacuolar programmed cell death. Bar = 2 µm

Scanning electron microscopy images

Pictures included several tissues for both MMS19 mutant and wild type. Leaves, anthers, and stems were observed under SEM. Results from leaves showed one consistent phenotype when compared to the wild type (Figure 11).

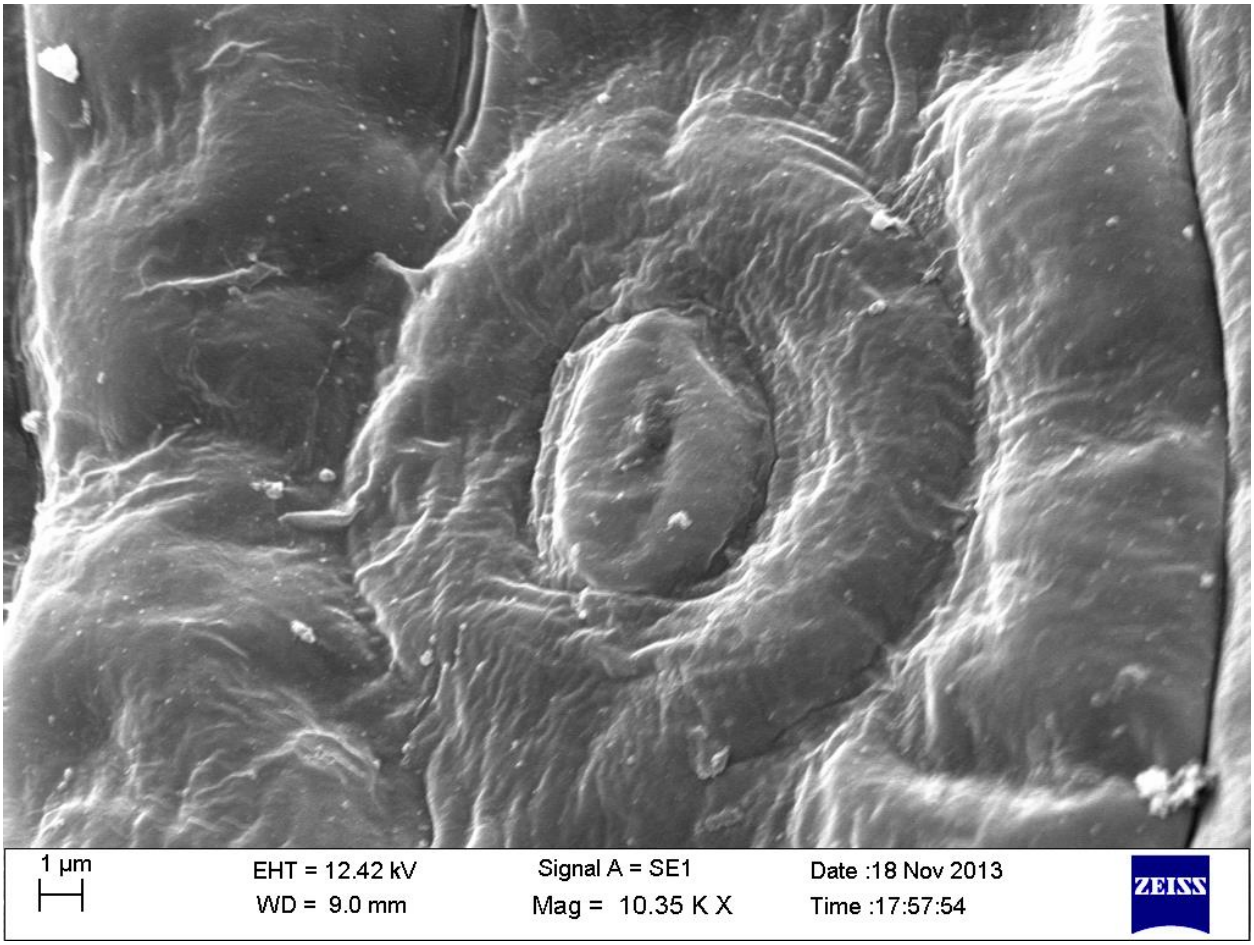

Figure 11 – Scanning electron microscope image of stomata and guard cells for MMS19 mutant.

During scanning of leaf epidermis for the MMS19 mutant, many stomata were visualized with this fused appearance.

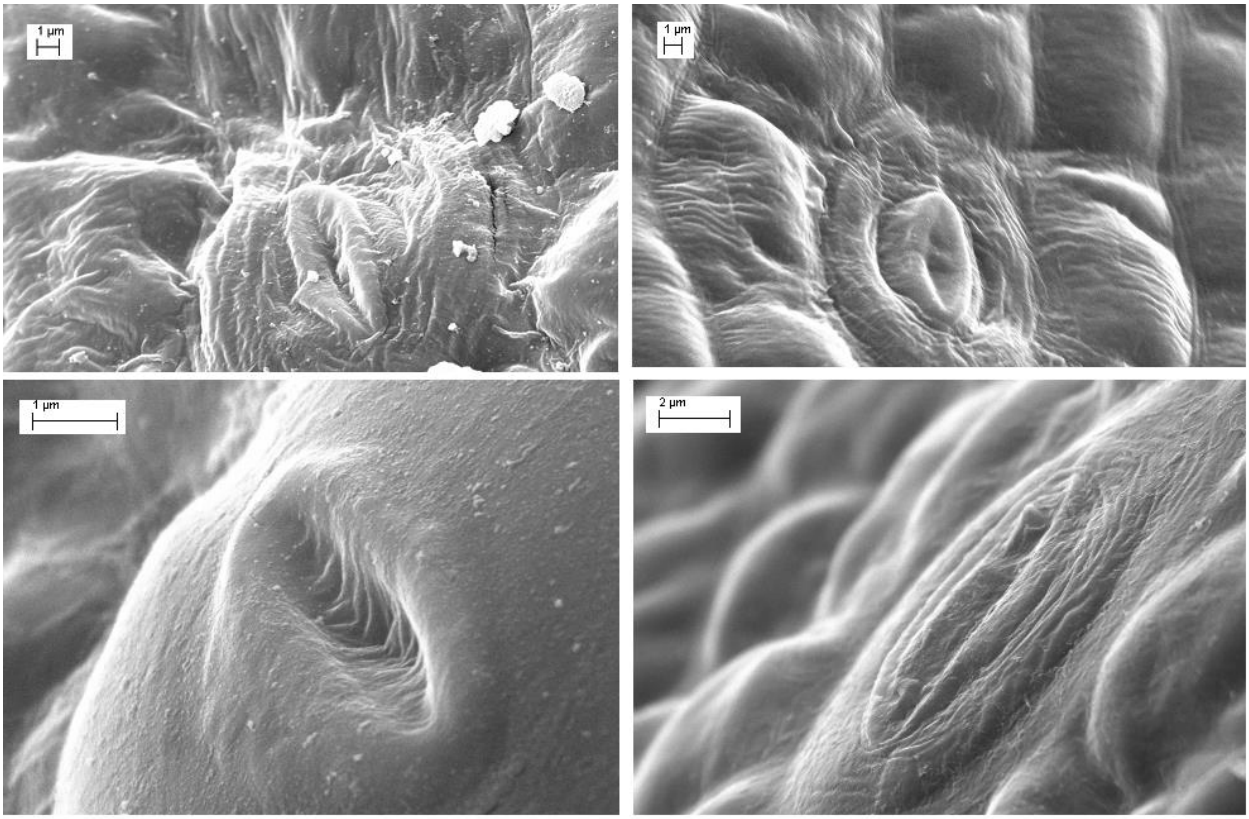

Figure 12 – Scanning electron microscope image of stomata within the epidermis of the MMS19 mutant leaves.

The fused guard cells within the stomata opening may be indicative of improper cell differentiation (Figure 12). By not forming the required supporting cells that are required by stomatal opening and closure the plant becomes limited in its access to water moisture and exchange of gases. Another possible explanation for this phenotype is that nuclear content within the guard cells has inherited mutations accrued by the previous cell's inefficient NER.

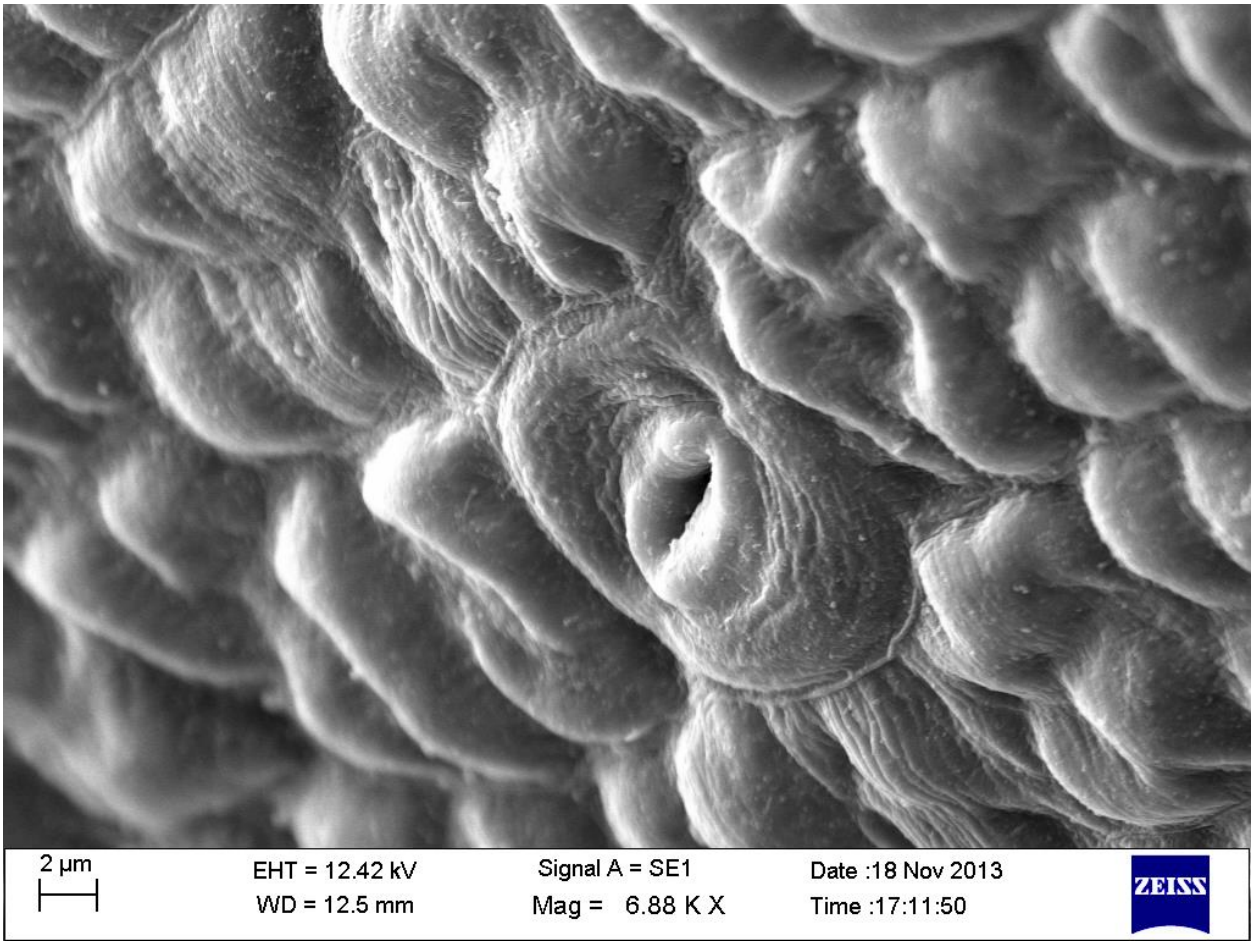

Figure 13 – Scanning electron microscope image of stomata on epidermis of wild type leaf.

What can be seen in the wild type are stomata with a well-defined opening for exchange of gases (Figure 13). Both of the leaf specimens chosen in this experiment were at the same developmental phase; young developing leaf tissues. Previous observations of leaf epidermis by Dr. Yu indicated to possible wrinkling of the cell wall epidermis for the MMS19 mutant. A comparison of two areas of the epidermis for the MMS19 mutant and the wild type reveal some wrinkling in young developing leaves for the mutant type (Figure 14).

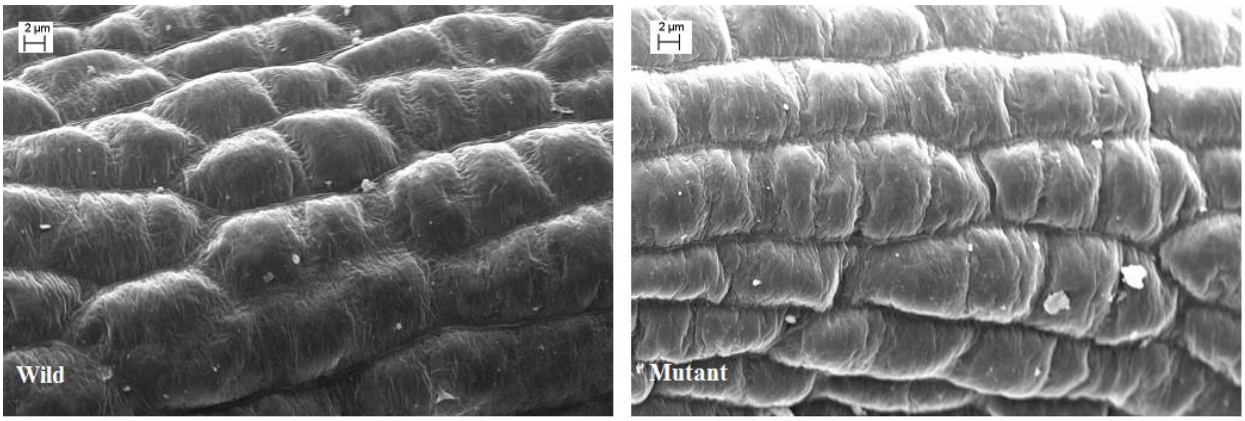

Figure 14 – Scanning electron microscope image of leaf epidermis for wild type and MMS19 mutant. Bar = 2 µm

Identification of alternative splice variants for MMS19

Research conducted at AgriLife Weslaco sought to identify specific binding of pre-designed primers for mutant and control tissues. It is known that within animal tissues MMS19 has several alternative splice variants that direct function of gene towards different cellular pathways (Hatfield 2006). In order to understand how MMS19 is expressed within wild and diminutive genotypes, different tissues were analyzed ranging from young and mature leaves to flowers. Quality of RNA eluted from extraction was tested and viewed under a UV transilluminator (Figure 15).

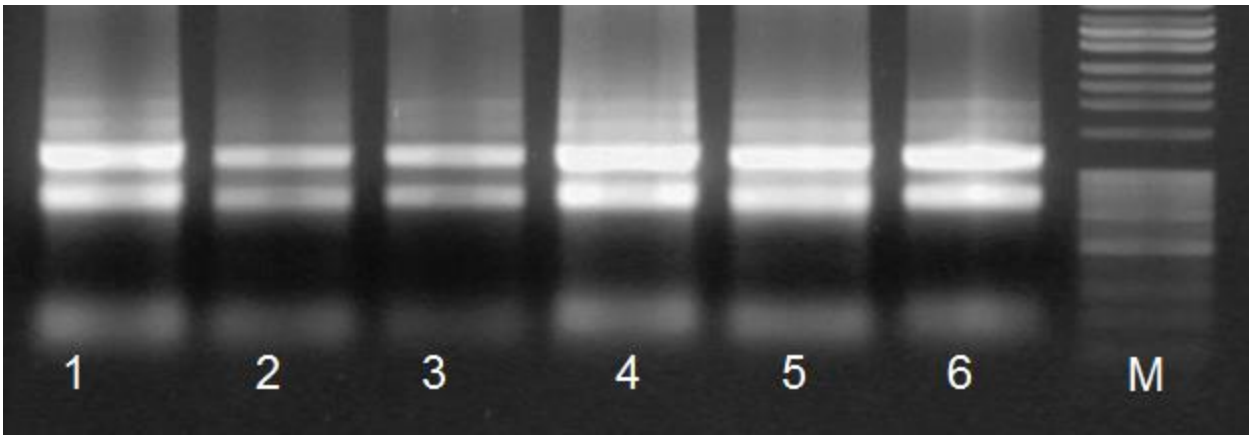

Figure 15 – Gel electrophoresis of *Carica papaya* tissues and markers. 1 – wild young leaf. 2- wild mature leaf. 3- wild flowers. 4- mutant young leaf. 5- mutant mature leaf. 6- mutant flowers. M – 1kb DNA ladder.

Some genomic contamination appeared in the young leaves when RNA extraction took place. Distinct RNA bands show that molecular transcripts separate into mRNA, tRNA and rRNA.. After cDNA was synthesized in a thermal cycler two sets of primers were aliquoted into master mixes to amplify and confirm the length of transcript for the diminutive and control type. In the diminutive plant, exons 9-18 have been functionally deleted as a result of a mutation. Two sets of primers were used to amplify the transcripts for both wild type and mutant.

PCR products from a modified reaction were electrophoresed on a new gel plate and clearly showed specific binding for the (+) control housekeeping gene CENH3 as well as very strong binding and amplification for the wild MMS19 tissue with primers (Figure 16).

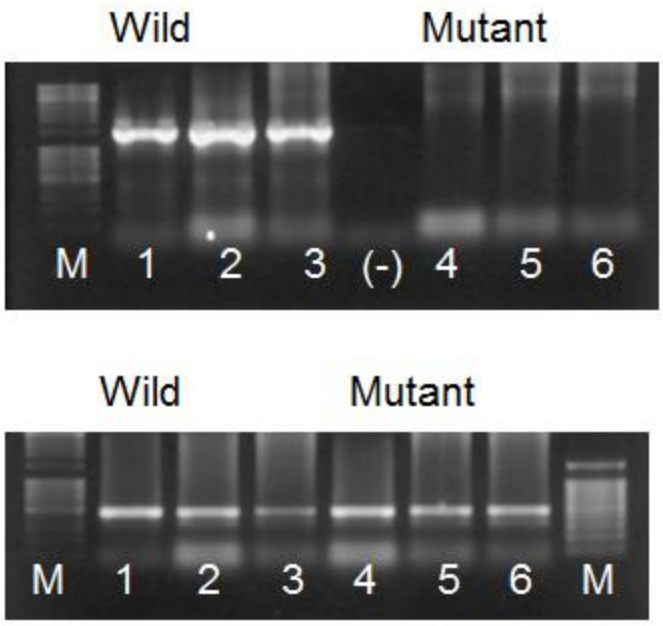

Figure 16 – Gel electrophoresis of wild, mutant, and CENH3 (+) control (bottom wells). TOP: 1-3 wild tissues, (-) negative control

A negative control was added to this gel to indicate whether primers had been contaminated and was amplifying the wild MMS19 gene products without the addition of cDNA. As there is no band in this negative control well, it can be assumed that there is no cDNA contamination within the primers. The size of the band produced for the wild type tissues in this gel is 1.5kbp's, fitting the predicted model. The (+) control with primers set for CENH3 cDNA is sized at 400 bp's, a good fit to the prediction as well. This uniform band formation across all tissues for both wild type and diminutive mutant clearly indicate that cDNA is present within the reaction, primers are not contaminated, and T.M. is optimized. The diminutive mutant tissues still show no band formation indicating that the PCR reaction for these primer sets and tissues is not amplifying cDNA molecules in the way they should. This in turn would later validate the observation that MMS19 gene within the diminutive mutant of *Carica papaya* has a functional

deletion in the exons 9-18, producing mRNA transcripts that do not have these coding regions. No observer was able to confirm that the primers designed for this experiment were inadequate for the diminutive MMS19 mutant as there was no way that the primer Cp_44 could bind to the exon-exon junction between 17-18. This oversight would cause the investigator to continue troubleshooting the PCR reaction attempting to amplify the diminutive transcript.

In the new reactions, the same primers are used for wild type and diminutive tissues. Same reverse primer of Cp 44- binding at the junction of exons 17 & 18, with cp40-F to the wild type and cp20-to the diminutive. No diminutive transcript appears to be amplified in the gel (Figure 16). There is the expected band of 1.5 kbp's for the wild type tissues. In young leaf and flower tissues (wells 3 & 4) there are other lightly stained bands for other transcripts that may have been amplified. There are included in the well a 1.0kbp and 300bp fragment. These may be naturally occurring alternative splice variants that have exons between 12-18 spliced out.
A new primer was chosen for amplification of tissues so as to trouble shoot the non-amplification of cDNA for the diminutive. Cp-35 as alternative splice detector was used for both MMS19 and diminutive tissues. What appears as very faint bands for the MMS19 tissues are a 1.5kbp band and in lower quantity a 1.0 kbp band. The binding of primer Cp-35 is to the first exon of the gene and in conjunction with cp 44 which binds the 18^{th} exon, would produce a megaband of >3.0kbp. As amplification of this amount of cDNA tends to decrease in efficiency, no bands would be expected. However the products visible on the gel hint to the possibility of some amplification of ASV's that exclude exons in range from 1-12, producing this reduced amplicon for the diminutive type.

Forward primer Cp20 and reverse primer Cp46 were tested and present in wells 5-7. In the MMS19 control tissues for primers producing an expected 3.4 kbp band there is a ~300 bp band with inconsistent expression across the tissues. The size and amount of transcript appears to be a product of chemically unstable PCR where template secondary structure may have interfered with proper elongation. Here, the sheer size of the desired product approaches limitation of reagents, as would be normal under long range PCR. In contrast, the diminutive tissues showed an amplified transcript measuring the estimated 841 bp's as had been done previously, confirming that the diminutive mRNA spans across the gene's functional deletion of exons 9-18.

Another primer set was chosen to confirm the same observation within diminutive tissues. As per the original forward primer Cp20 was used for both wild type and diminutive tissues. Reverse primer was Cp46 for both types of tissues. For the wild type, an expected band size of 3.0 kbp was predicted. No reaction took place as the wells show clearly that no amplification of product took place. For the diminutive tissues in the bottom wells, there is band of approximately ~500 bp, confirming the predicted 548 bp product from this reaction. This reaction proves interesting as there is a clear band present for the mature type tissues within the diminutive that possibly exclude mRNA transcripts with the upstream exons 1-5. These upstream exons are included with the alternative splicing of exon 2 for the 841bp amplicon found for the other primer set in this gel. This coincides with the prediction from other journals that cite the A-domain within the N-terminus of the polypeptide as directing function towards TFIIH activity (Figure 17). When present, the A domain may confer stability of TFIIH to function in a RNA II Pol dependent manner, facilitating the production of genes necessary for cellular division and growth as this domain is not found active in mature tissues. Where the B domain that directs

function of TFIIH for DNA repair, this product appears more present in developing leaves, but is also present in mature leaves and flowers. This makes sense as DNA repair is fundamental part of all cellular function at any stage.

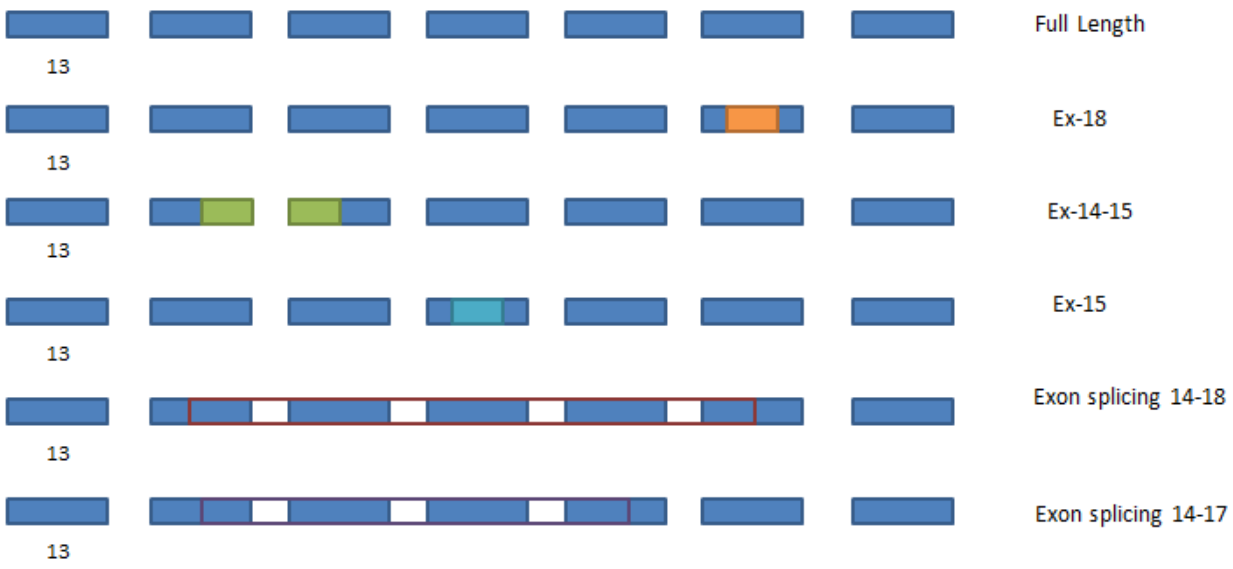

Figure 17 – Graph illustrating the areas where alternative splicing is hypothesized to occur in the MMS19 wild type.

Identification of putative orthologs for NER related genes

MMS19 has been linked extensively to Nucleotide Excision Repair in eukaryotes. The protein however is not directly involved in DNA damage repair. Studies in yeast and humans have shown that mms19 is involved in maintaining adequate amounts of XPD and XPB helicases required for TFIIH function in both DNA damage repair and RNA Pol II transcription. In *Arabidopsis*, MET18 (mms19) was co-immunoprecipitated alongside several other proteins involved in Cytosolic Iron Sulfur Cluster Assembly (CIA) machinery. Knock out mutants for this gene showed no distinct phenotypes, but when multiple CIA proteins were knocked out, embryo

lethality was increased. In an effort to discover the role of mms19 in papaya, gene expression analysis of downstream events correlated with mms19 would be conducted.

Eight homologous genes were identified in papaya. Six of these are involved in NER ranging from identification of damaged DNA to unwinding of the damaged portion of the double helix. In order for these proteins to anchor correctly to DNA they must have an inorganic Fe-S bridge.

It was proposed that if an mms19 mutation were to decrease the availability of Fe-S clusters to NER proteins, more DNA damage would accumulate and thereby decrease cell proliferation. There would also be an increase in expression of NER repair genes. Semiquantitative analysis revealed that a majority of downstream genes involved in NER did not show an increase in expression (See Figure 18). However, a near two-fold increase in XPC (a DNA damage recognition enzyme) occurred in mms19 mutant. A similar two-fold increase in WEE1 (cell cycle kinase) was observed in the mms19 mutant, indicating that cell division could be negatively affected by accumulation of DNA damage (See Figure 18A). These increases do not represent drastic changes in overall gene expression when compared to other mutants who are deficient in CIA machinery. However, these observations may help explain why the diminutive mutant has decreased growth compared to its wild type counterpart. In conclusion, mms19 may be linked to DNA metabolism but is not integral in maintaining genomic integrity.

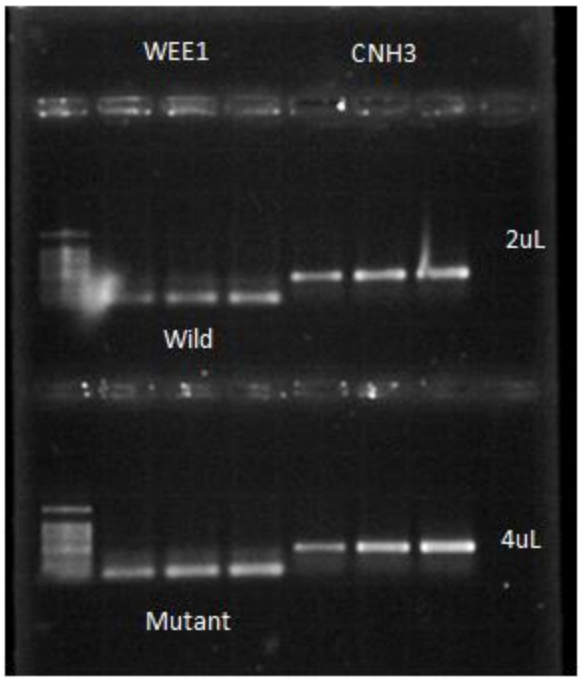

Figure 18 - Semiquantitative PCR of WEE1-kinase, responsible for DNA integrity cell cycle arrest checkpoint.

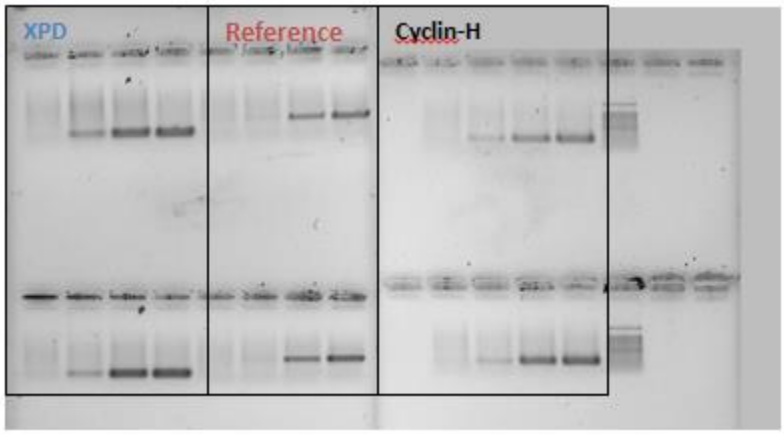

Figure 18A. Semiquantitative PCR of TFIIH components XPD helicase and Cyclin-H. No noticeable increase in expression.

Quantitation of mRNA levels for NER related genes

qRT-PCR proved successful after analyzing critical threshold levels for 7 of the 8 genes of interest. Using the Pfaffl equation to quantify relative levels of mRNA, a graph was created to show the down or up regulation occurring within the target MMS19 mutant (Figure 19). All levels displayed for the mutant are expressed as ratios to the wild type control. The genes of interest can be divided into three groups. XPD, XPC, and XPB are gene homologs that are hypothesized to be apoproteins stabilized by the MMS19 scaffolding complex. None of the helicases show any significant amount of alteration in their profile.

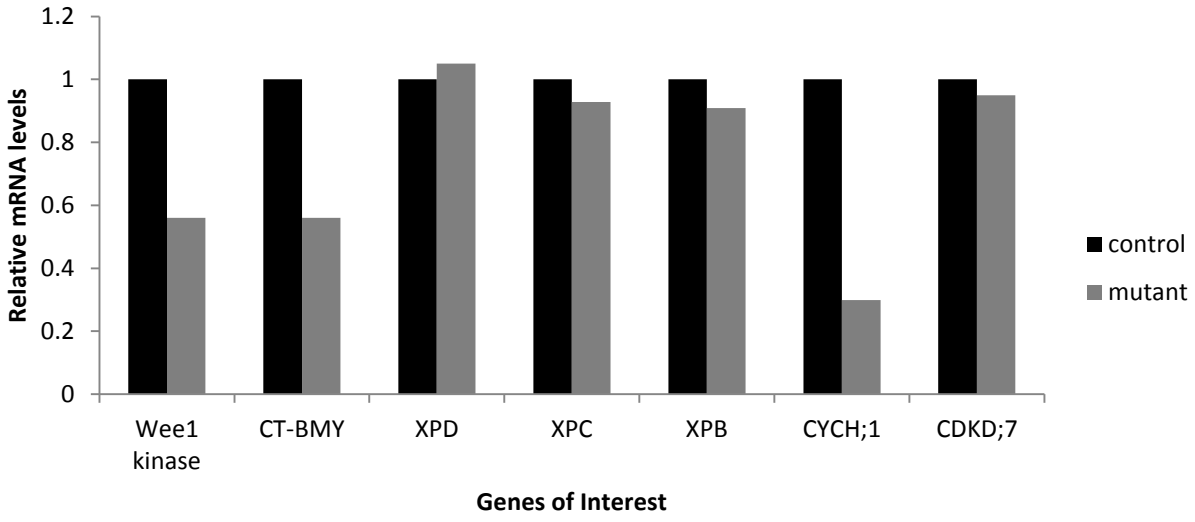

Figure 19 – Relative quantitation of mRNA for MMS19 diminutive mutant

The other group of genes studied include the CAK complex (cyclin-dependent activating kinase) CYCH;1 and CDKD;7. Although CDKD;7 does not show any difference in mRNA profile, CYCH;1 shows a considerable down regulation of 1/3rd ratio to the wild type. These are genes that are associated with the core TFIIH holocomplex involved in TC-NER and GG-NER.

The final group of genes includes Wee1 kinase and CT-BMY. Wee1 is a cell cycle control gene that regulates entry into mitosis. This gene is down regulated twofold (1/2) in the

mutant. CT-BMY is a chloroplast-targeting β-amylase. This gene also shows a twofold down regulation (1/2) in the MMS19 mutant.

To verify the proper amplification of desired products a gel was electrophoresed with all the samples from the qRT-PCR reaction.

Fluorescent staining of nuclei using confocal microscopy

The morphology of each leaf for this species shows two distinct layers to the tissue, the palisade parenchyma and spongy mesophyll. Staining of nuclei with Hoechst 33342 revealed several distinct differences between the wild type and MMS19 mutant. As can be observed in Figure 20 the nuclear content of the wild type is numerous and prolific across the leaf. In the mutant the number of nuclei and distribution is significantly less.

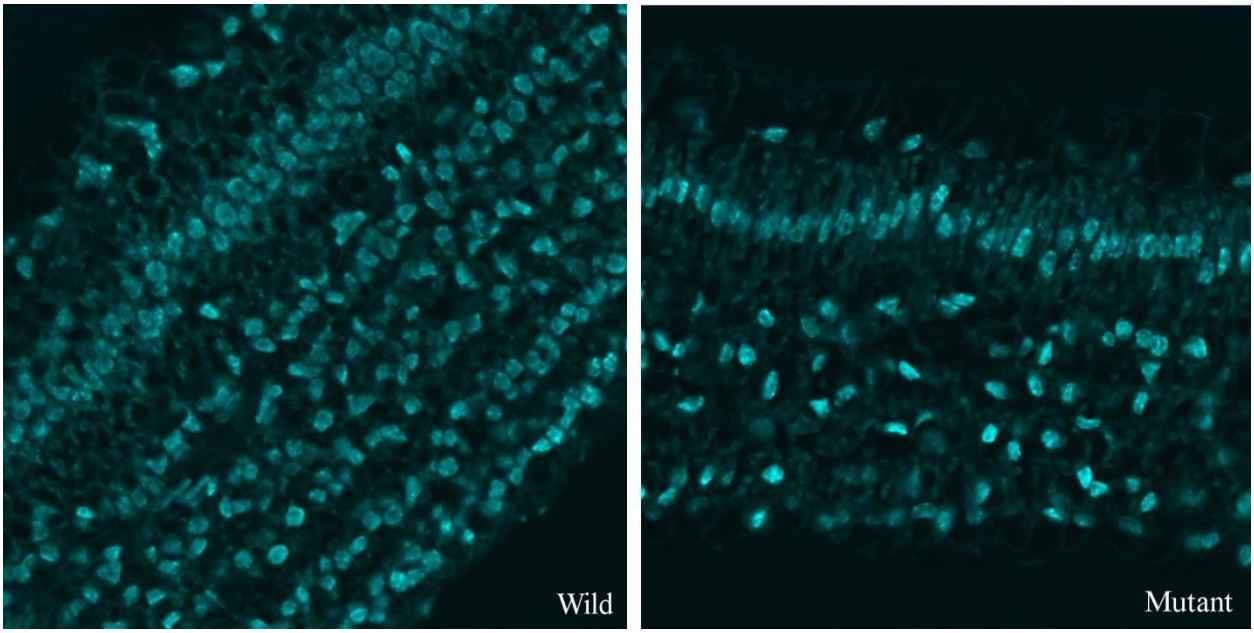

Figure 20 – Laser scanning confocal image of papaya leaves stained with Hoechst 33342. Magnification = 600x

Two leaves at the same developmental stage of approximately 7 months show the beginning onsets of what could be described as retarded growth for the MMS19 mutant. Where it is clearly visible that the wild type leaf shows a well-developed palisade parenchyma (upper layer of vertical cells), the mutant's palisade appears to be reduced in volume and compressed. The spongy mesophyll (lower cell layer) of the wild type leaf has a high number of nucleated cells as evidenced by the high fluorescent signal produced. Quantification of the number of nucleated cells revealed that the wild type indeed has a higher number of viable cells at the same developmental stage as the MMS19 mutant (See Figure 20A).

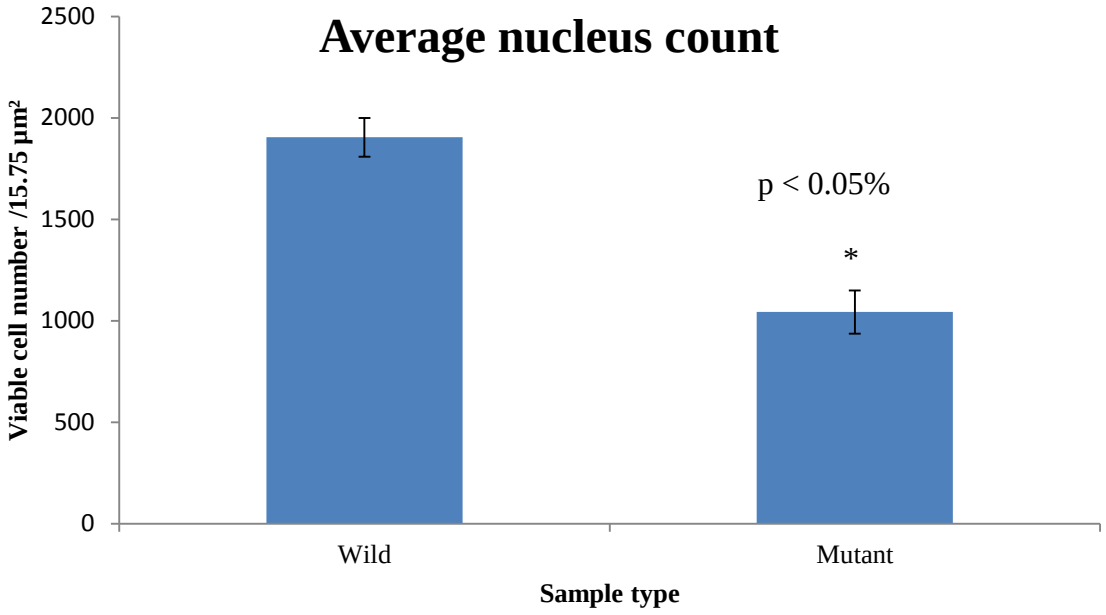

Figure 20A – Number of cells counted by nuclear fluorescent signal

Cell viability was assayed as the number of visible nucleated signals arising from the tissue sample. The wild type image revealed to have an average 1,904 cells and the MMS19 mutant showed 1,043. This confirms that the MMS19 mutant type leaf has fewer total viable cells during development when compared to the wild type.

Immunogold labeling of MMS19

After sections were treated with the MMS19 primary antibody and conjugated with gold particles, they were viewed under the transmission electron microscope. Although this experiment was conducted twice and with a negative control, it is difficult to assess whether the primary antibody is specifically binding to the desired epitope. Figure 21 shows the negative control with no primary antibody added to the reaction indicating no non-specific binding. There is clearly no evidence of gold particles conjugating randomly.

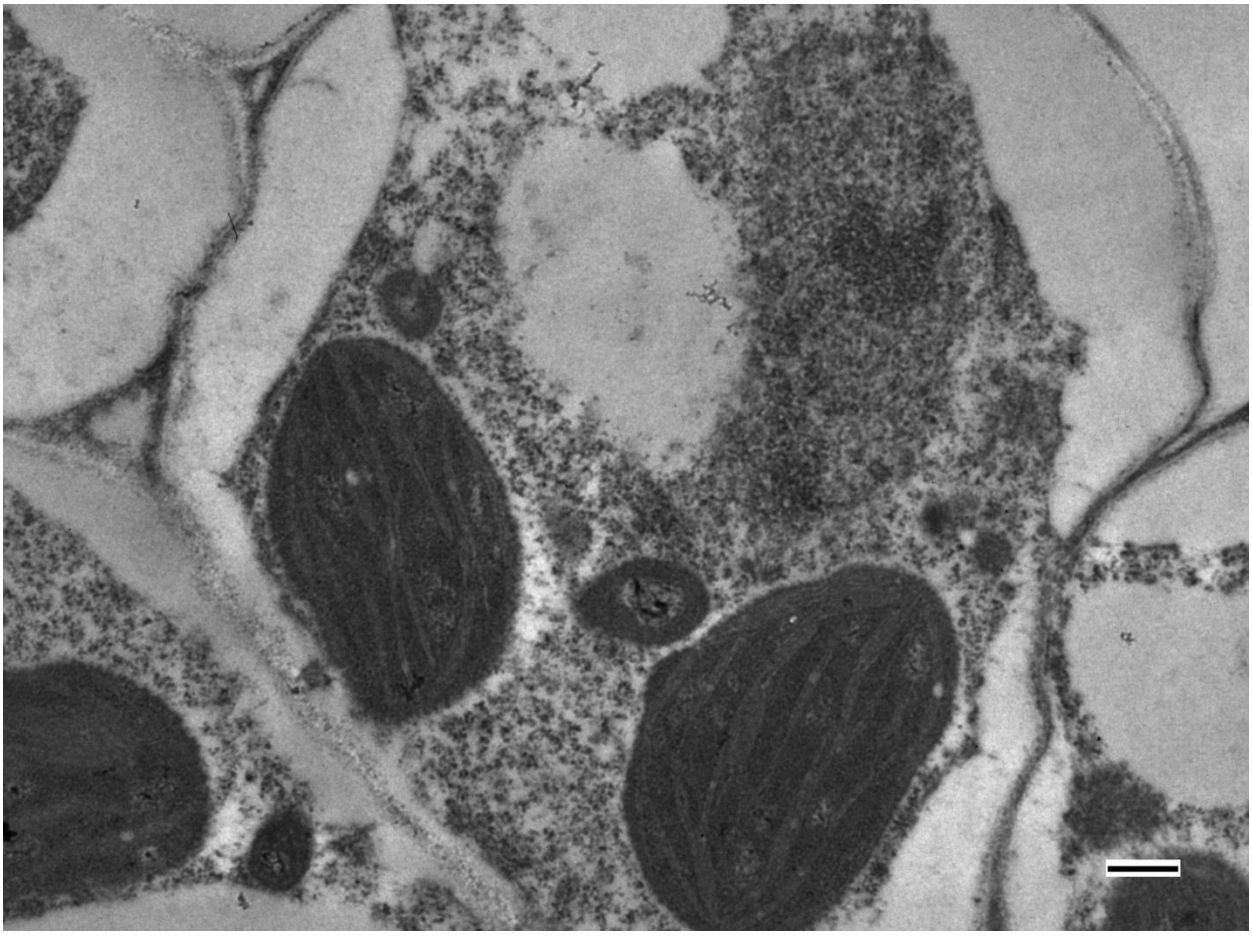

Figure 21 – TEM micrograph of wild type papaya leaf with no primary antibody added to immunolocalization experiment. Bar = 500 nm

In another image captured, the wild type leaf cells show that MMS19 is ubiquitously found within the cell, including the cytoplasm and nucleus. In comparison to the wild type, the MMS19 mutant type shows increased amount of MMS19 localized to the vacuole (Figure 22).

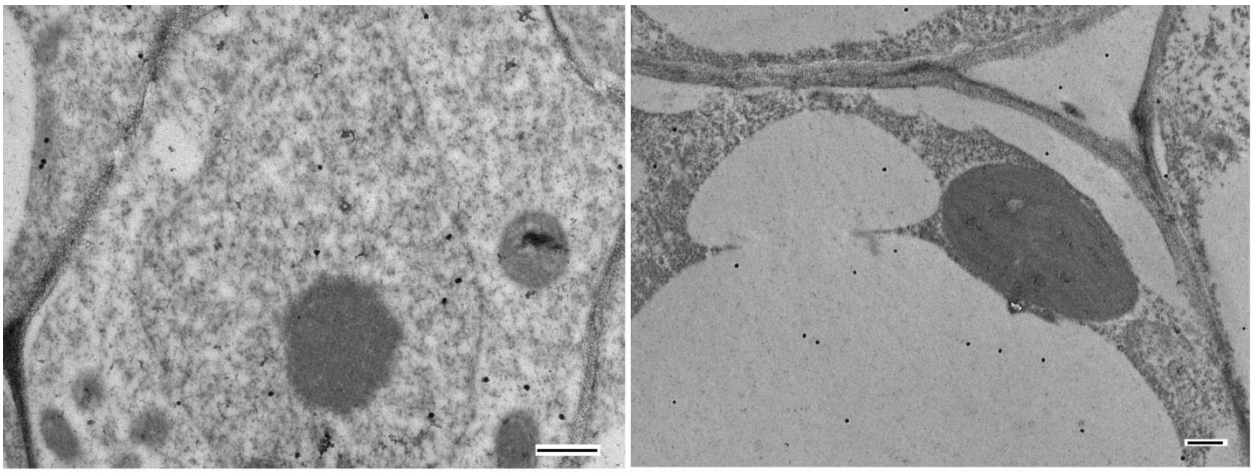

Figure 22 – TEM micrograph of wild type and mutant papaya leafs with immunogold labeling. Bar on left = 500 nm, on right = 500 nm

CHAPTER V

DISCUSSION

The original hypothesis suggested by the researcher implicated MMS19 as a crucial factor for functional NER (Yu, 2014). Upon subsequent investigation, MMS19 appeared to function in more ways than in its indirect maintenance of crucial TFIIH subunits. Growth and development appear to be affected negatively by MMS19 deficiency as well as telomere maintenance. With this premise in mind, the researcher attempted to identify consistent phenotypic differences within the MMS19 mutant when compared to the wild type. The primary focus of light and electron microscopy was to scan selected tissues for interesting morphological differences. Electron microscopy results indicated that the MMS19 mutant undergoes significant physiological changes when compared to the wild type. At the cellular level the MMS19 mutant shows a drastic increase in autolytic activity within the vacuole. Along with this an increased amount of plant-like apoptotic activity was noted in cells undergoing development within young tissues. In mature leaves the upper epidermis of the mutant type showed large amounts of cell death through necrosis, leading to a collapsed cell wall. Autophagic activity by perixosomes and lysosomes show mitochondria being absorbed for degradation within the mutant. Accumulation of starch grains within the chloroplast also shows a possible metabolic difference between the mutant and wild type. Some light microscopy images also revealed inconsistent vascular differentiation within tissues like leaves. All of these features are in support of the idea that inefficient DNA repair mechanisms play a significant role in normal plant physiology. Although

several studies have shown that MMS19 deficient mutants show growth deficiencies along with heat sensitivity, there is no current study that elaborates so many physical attributes to the MMS19 mutation within higher plants.

Alternative splicing primers revealed that exon splicing does occur in mms19. Exons 14-18 show significant amounts of splicing. Exon splicing also occurs between exons 2-3. It is possible that the C-terminal domain of MMS19 undergoes alternative splicing to preferentially direct MMS19's function. Splice variants identified in humans and mice indicate that mms19 activity can be coordinated between NER and RNA Pol II activity. However it has been noted in yeast that the C-terminal HEAT repeat sequence in mms19 is necessary for the transfer of Fe-S clusters to NER proteins.

Diminutive mms19 mutant has exons 9-18 deleted. The C-Terminal domain with conserved HEAT repeats is affected by this mutation and would alter the scaffolding capabilities of mms19 in the CIA machinery. Cloning the mms19 diminutive sequence and functional complementation to yeast would show the extent to which the truncated region affects UV-radiation sensitivity, mms treatment, and temperature treatments.

To further elucidate the roles of alternative splice variants for mms19, functional complementation and western blot analysis may reveal the extent to which mms19 encodes structurally and functionally distinct protein products.

MMS19 has been implicated as an upstream regulator of TFIIH activity (Gari, 2012). XPD, XPC, and XPB are helicases that sense damage in GG-NER and assist in TC-NER by targeting lesions across DNA. As per literature citing that CAK related genes and XPD are differentially affected in their association to core TFIIH during NER (Arab 2010), these results show that MMS19 deficiency does not trigger the downstream down/up regulation of XPD.

There is however an observable decrease in one CAK complex gene, CYCH;1 that shows a remarkable 1/3rd decrease in mRNA. This may indicate that CYCH;1 is downstream regulated by functional MMS19. What could be occurring with the XPD, XPC and XPB genes is that the ATM (Ataxia Telangectiesaia Mutated) damage sensing pathway is triggering the expression of these genes at normal levels. Another hypothesis includes that CYCH;1 is down regulated as part of a drought-resistance phenotype observed in *Arabidopsis* (Zhou 2013). This observation is corroborated by the overall water deficient phenotype associated with chloroplast starch accumulation and lack of vascular differentiation.

The down regulation of wee1 kinase is a key sign of an altered physiological profile affected by the MMS19 mutation. This gene acts as a DNA integrity checkpoint kinase that phosphorylates CDK's into an inactive state, pausing cell cycle progression before mitosis. The benefit of this gene is to make sure that any lesions or damage accumulated in the genome is corrected before DNA is replicated and the mitotic cell cycle begins. The two fold reduction in availability of mRNA for this gene indicates that fewer cells are undergoing the DNA integrity checkpoint in the MMS19 mutant. An explanation of this phenomenon could be that reduced NER proficiency will in turn increase the amount of cell cycle aborts within the organism's development. If DNA repair mechanisms cannot fix lesions such as cyclobutane-pyrimidine dimers that are preferentially targeted by TC-NER or GG-NER mechanisms, affected cells will reach an end phase in their life cycle (Figure 23). Differentiation into other cellular types will be negatively affected and cell proliferation will decrease. Another genomic effect that will occur as a result of unrepaired lesions is that of translesion synthesis (Cools, 2011). Translesion synthesis occurs when genes are synthesized by specialized DNA polymerases that carry lower fidelity during replication. The insertion of mismatched bases will sometimes result in the creation of

pseudo or non-functional genes within the genome (Hays 2002). This could explain the prevalence of pseudo-functional stomata and irregular growth patterns exhibited by the MMS19 mutant.

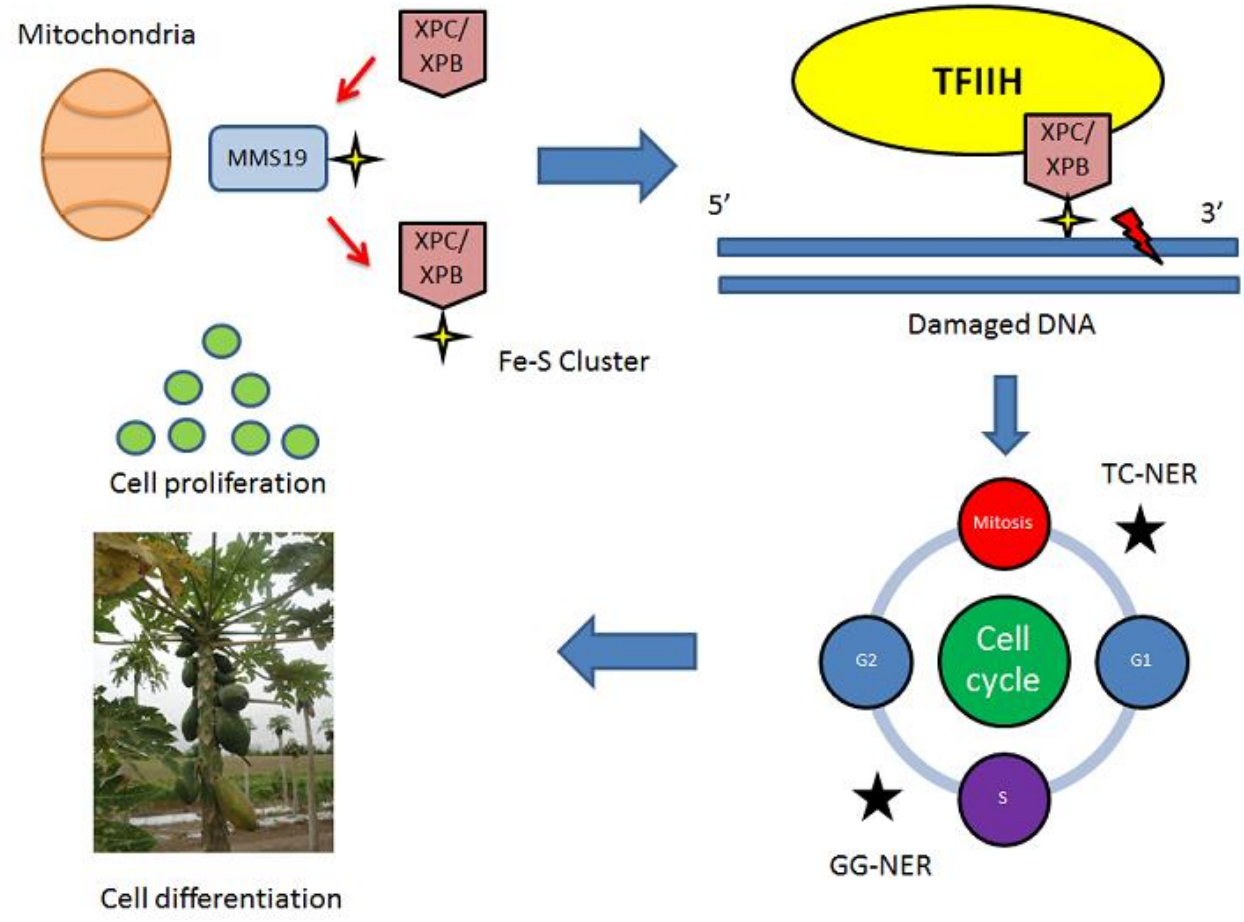

Figure 23 – MMS19 indirectly linked to maintaining adequate cellular proliferation and differentiation across tissues in plants.

The cumulative effects of these genomic alterations will overtime produce a diminutive phenotype where a majority of tissues show some reduction in size and growth rate. These are in fact some of the originally observed phenotypes associated with the MMS19 diminutive mutant, conferred now by transcriptional analysis.

CT-BMY is a chloroplast targeting b-amylase that is nuclear encoded and travels to the plastid within plants to assist in liberation and digestion of starch molecules for metabolic respiration. The two fold reduction in this gene's mRNA signifies a reduced amount of enzyme present within the cell localizing to the chloroplast for starch degradation. Normally plants undergo constant remobilization of starch reserves formed during a photoperiod to provide energy for metabolic processes. As was noted in several light and electron microscopic images, a very clear starch accumulation phenotype was occurring in the MMS19 mutant. The phenotype is now confirmed with a transcriptional profile that helps explain the increasing size of starch grains within chloroplasts as a direct result of decreased CT-BMY present within cells.

There are several hypotheses that might explain the increased accumulation of starch grains within chloroplasts. One of primary interest to the researcher is that through the observed decrease in cell proliferation and differentiation, less energy is needed for mitotic divisions. Mitosis is a costly part of a cell's cycle (Eisenberg 2011) that requires a large amount of free energy for duplication processes. As cells become shunted away from mitotic progression, they enter an end point phase that will require less energy consumption when compared to a still dividing wild type cell.

Depending on which domain of the gene is preferentially expressed, MMS19 will either enter into a transcription or NER dominant form. When the MMS19 deletion mutant transcript is expressed, the domain consisting of exons 9-18 will be absent, inhibiting preferential expression patterns. The 4-HEAT repeat sequences in MMS19 are conserved across species and are believed to be essential for proper NER function (Luo 2012). Because the C-terminal domain where the 4-HEAT repeat sequences are found is missing large sections of coding material, it can be assumed that NER dependent expression will be affected.

Images from all of the electron and light microscopy experiments consistently revealed a phenotype for the mutant that exhibited increased autolytic and apopototic activity. By confirming the observed differences in morphology with molecular data, the researcher was able to implicate several transcriptional profiles as affected by the MMS19 mutation. Investigative analysis sought to explain how the increased amount of cellular death and cell cycle arrest within the mutant might result in creating the diminutive phenotype. Water transport was identified as a possible explanation to this, as inefficient circulation of water through the xylem tissues would in turn affect metabolism and rate of growth. Growth itself is also affected indirectly by the MMS19 mutation, as the TFIIH complex so necessary for RNA II Pol function is hypothesized to be nonfunctional. Future investigations would require protemic analysis of this holocomplex to see if the MMS19 linked proteins XPD and XPB are in fact not well associated to the repair complex. Inefficient nucleotide excision repair would overtime lead to the accumulation of deleterious mutation within the genome. One possibility that could be investigated would be to precipitate histone proteins to identify any possible single strand breaks or double strand breaks within the genome.

REFERENCES

Agriculture, H. (2000). PRODUCTION OF UH SUNUP TRANSGENIC PAPAYA SEED IN HAWAII, (October).

Aksoy, E., Jeong, I. S., & Koiwa, H. (2013). Loss of function of *Arabidopsis* C-terminal domain phosphatase-like1 activates iron deficiency responses at the transcriptional level. *Plant Physiology*, *161*(1), 330–45. http://doi.org/10.1104/pp.112.207043

Arab, H. H., Wani, G., Ray, A., Shah, Z. I., Zhu, Q., & Wani, A. a. (2010). Dissociation of CAK from core TFIIH reveals a functional link between XP-G/CS and the TFIIH Disassembly State. *PLoS ONE*, *5*(6). http://doi.org/10.1371/journal.pone.0011007

Askree, S. H., Yehuda, T., Smolikov, S., Gurevich, R., Hawk, J., Coker, C., … McEachern, M. J. (2004). A genome-wide screen for *Saccharomyces cerevisiae* deletion mutants that affect telomere length. *Proceedings of the National Academy of Sciences of the United States of America*, *101*(23), 8658–8663. http://doi.org/10.1073/pnas.0401263101

Bieza, K., & Lois, R. (2001). An Arabidopsis Mutant Tolerant to Lethal Ultraviolet-B Levels Shows Constitutively Elevated Accumulation of Flavonoids and Other Phenolics 1, *126*(July), 1105–1115.

Budden, T., & Bowden, N. a. (2013). The Role of Altered Nucleotide Excision Repair and UVB-Induced DNA Damage in Melanomagenesis. *International Journal of Molecular Sciences*, *14*(1), 1132–51. http://doi.org/10.3390/ijms14011132

Cook, G. S., Grønlund, A. L., Siciliano, I., Spadafora, N., Amini, M., Herbert, R. J., … Rogers, H. J. (2013). Plant WEE1 kinase is cell cycle regulated and removed at mitosis via the 26S proteasome machinery. *Journal of Experimental Botany*, *64*(7), 2093–2106. http://doi.org/10.1093/jxb/ert066

Cools, T., Iantcheva, A., Weimer, A. K., Boens, S., Takahashi, N., Maes, S., … De Veylder, L. (2011). The *Arabidopsis thaliana* checkpoint kinase WEE1 protects against premature vascular differentiation during replication stress. *The Plant Cell*, *23*(4), 1435–1448. http://doi.org/10.1105/tpc.110.082768

De Schutter, K., Joubès, J., Cools, T., Verkest, A., Corellou, F., Babiychuk, E., … De Veylder, L. (2007). *Arabidopsis* WEE1 kinase controls cell cycle arrest in response to activation of the DNA integrity checkpoint. *The Plant Cell*, *19*(1), 211–25. http://doi.org/10.1105/tpc.106.045047

Eisenberg, D. T. a. (2011). An evolutionary review of human telomere biology: The thrifty telomere hypothesis and notes on potential adaptive paternal effects. *American Journal of Human Biology*, *23*(2), 149–167. http://doi.org/10.1002/ajhb.21127

Fidantsef, A. L., Mitchell, D. L., Britt, A. B., Biology, P., & California, A. L. F. (2000). The *Arabidopsis* UVH1 Gene Is a Homolog of the Yeast Repair Endonuclease RAD1 1, *124*(October), 579–586.

Hara-Nishimura, I., & Hatsugai, N. (2011). The role of vacuole in plant cell death. *Cell Death and Differentiation*, *18*(8), 1298–1304. http://doi.org/10.1038/cdd.2011.70

Gari, K., Leon Ortiz, a. M., Borel, V., Flynn, H., Skehel, J. M., & Boulton, S. J. (2012). MMS19 Links Cytoplasmic Iron-Sulfur Cluster Assembly to DNA Metabolism. *Science*, *337*(6091), 243–245. http://doi.org/10.1126/science.1219664

Hatfield, M. D., Reis, A. M. C., Obeso, D., Cook, J. R., Thompson, D. M., Rao, M., … Queimado, L. (2006). Identification of MMS19 domains with distinct functions in NER and transcription. *DNA Repair*, *5*(8), 914–24. http://doi.org/10.1016/j.dnarep.2006.05.007

Hays, J. B. (2002). Arabidopsis thaliana, a versatile model system for study of eukaryotic genome-maintenance functions. *DNA Repair*, *1*(8), 579–600. http://doi.org/10.1016/S1568-7864(02)00093-9

Hollósy, F. (2002). Effects of ultraviolet radiation on plant cells. *Micron*, *33*. Retrieved from http://www.sciencedirect.com/science/article/pii/S0968432801000117

Jiang, L., Wang, Y., Björn, L. O., & Li, S. (2014). Does cell cycle arrest occur in plant under solar UV-B radiation? *Plant Signaling & Behavior*, *6*(6), 892–894. http://doi.org/10.4161/psb.6.6.15317

Kamileri, I., Karakasilioti, I., & Garinis, G. a. (2012). Nucleotide excision repair: new tricks with old bricks. *Trends in Genetics : TIG*, *28*(11), 566–73. http://doi.org/10.1016/j.tig.2012.06.004

Kou, H., Zhou, Y., Gorospe, R. M. C., & Wang, Z. (2008). Mms19 protein functions in nucleotide excision repair by sustaining an adequate cellular concentration of the TFIIH component Rad3. *Proceedings of the National Academy of Sciences of the United States of America*, *105*(41), 15714–9. http://doi.org/10.1073/pnas.0710736105

Krizek, D. T. (2004). Invited Review Influence of PAR and UV-A in Determining Plant Sensitivity and Photomorphogenic Responses to UV-B Radiationqt, *79*(4).

Kunz, B. a, Anderson, H. J., Osmond, M. J., & Vonarx, E. J. (2005). Components of nucleotide excision repair and DNA damage tolerance in Arabidopsis thaliana. *Environmental and Molecular Mutagenesis*, *45*(2-3), 115–27. http://doi.org/10.1002/em.20094

Laat, W. L. De, Jaspers, N. G. J., & Hoeijmakers, J. H. J. (1999). Molecular mechanism of nucleotide excision repair Molecular mechanism of nucleotide excision repair, 768–785.

Larsen, N. B., Rasmussen, M., & Rasmussen, L. J. (2005). Nuclear and mitochondrial DNA repair: similar pathways? *Mitochondrion*, *5*(2), 89–108. http://doi.org/10.1016/j.mito.2005.02.002

Lauder, S., Bankmann, M., Guzder, S. N., Sung, P., Prakash, L., & Prakash, S. (1996). Dual Requirement for the Yeast MMS19 Gene in DNA Repair and RNA Polymerase II Transcription, *16*(12), 6783–6793.

Li, A., Schuermann, D., Gallego, F., Kovalchuk, I., & Tinland, B. (2002). Repair of Damaged DNA by *Arabidopsis* Cell Extract, *14*(January), 263–273. http://doi.org/10.1105/tpc.010258.and

Light, U., & Dimers, P. (2001). O ncologist The Molecular Perspective : Ultraviolet Light and Pyrimidine Dimers, 298–299.

Lill, R., Dutkiewicz, R., Elsässer, H. P., Hausmann, A., Netz, D. J. a, Pierik, A. J., … Mühlenhoff, U. (2006). Mechanisms of iron-sulfur protein maturation in mitochondria, cytosol and nucleus of eukaryotes. *Biochimica et Biophysica Acta - Molecular Cell Research*, *1763*(7), 652–667. http://doi.org/10.1016/j.bbamcr.2006.05.011

Lill, R., Hoffmann, B., Molik, S., Pierik, A. J., Rietzschel, N., Stehling, O., … Mühlenhoff, U. (2012). The role of mitochondria in cellular iron-sulfur protein biogenesis and iron metabolism. *Biochimica et Biophysica Acta - Molecular Cell Research*, *1823*(9), 1491–1508. http://doi.org/10.1016/j.bbamcr.2012.05.009

Liu, Z., Hossain, G. S., Islas-Osuna, M. a., Mitchell, D. L., & Mount, D. W. (2000). Repair of UV damage in plants by nucleotide excision repair: *Arabidopsis* UVH1 DNA repair gene is a homolog of Saccharomyces cerevisiae Rad1. *The Plant Journal*, *21*(6), 519–528. http://doi.org/10.1046/j.1365-313x.2000.00707.x

Livak, K. J., & Schmittgen, T. D. (2001). Analysis of relative gene expression data using real-time quantitative PCR and the 2(-Delta Delta C(T)) Method. *Methods (San Diego, Calif.)*, *25*(4), 402–8. http://doi.org/10.1006/meth.2001.1262

Lombaerts, M., Tijsterman, M., Verhage, R. a., & Brouwer, J. (1997). *Saccharomyces cerevisiae* mms19 mutants are deficient in transcription-coupled and global nucleotide excision repair. *Nucleic Acids Research*, *25*(20), 3974–3979.

Lundin, C., North, M., Erixon, K., Walters, K., Jenssen, D., Goldman, A. S. H., & Helleday, T. (2005). Methyl methanesulfonate (MMS) produces heat-labile DNA damage but no detectable in vivo DNA double-strand breaks. *Nucleic Acids Research*, *33*(12), 3799–3811. http://doi.org/10.1093/nar/gki681

Luo, D., Bernard, D. G., Balk, J., Hai, H., & Cui, X. (2012). The DUF59 family gene AE7 acts in the cytosolic iron-sulfur cluster assembly pathway to maintain nuclear genome integrity in *Arabidopsis*. *The Plant Cell*, *24*(10), 4135–48. http://doi.org/10.1105/tpc.112.102608

Matsuno, M., Kose, H., Okabe, M., & Hiromi, Y. (2007). TFIIH controls developmentally-regulated cell cycle progression as a holocomplex. *Genes to Cells : Devoted to Molecular & Cellular Mechanisms*, *12*(11), 1289–300. http://doi.org/10.1111/j.1365-2443.2007.01133.x

Meyer, J. (2008). Iron-sulfur protein folds, iron-sulfur chemistry, and evolution. *Journal of Biological Inorganic Chemistry*, *13*(2), 157–170. http://doi.org/10.1007/s00775-007-0318-7

Ming, R., Hou, S., Feng, Y., Yu, Q., Dionne-Laporte, A., Saw, J. H., … Alam, M. (2008). The draft genome of the transgenic tropical fruit tree papaya (*Carica papaya* Linnaeus). *Nature*, *452*(7190), 991–6. http://doi.org/10.1038/nature06856

Molinier, J., Ramos, C., Fritsch, O., & Hohn, B. (2004). CENTRIN2 modulates homologous recombination and nucleotide excision repair in *Arabidopsis*. *The Plant Cell*, *16*(6), 1633–43. http://doi.org/10.1105/tpc.021378

Morgante, P. G., Berra, C. M., Nakabashi, M., Costa, R. M. a, Menck, C. F. M., & Van Sluys, M.-A. (2005). Functional XPB/RAD25 redundancy in *Arabidopsis* genome: characterization of AtXPB2 and expression analysis. *Gene*, *344*, 93–103. http://doi.org/10.1016/j.gene.2004.10.006

Nelissen, H., De Groeve, S., Fleury, D., Neyt, P., Bruno, L., Bitonti, M. B., … Van Lijsebettens, M. (2010). Plant Elongator regulates auxin-related genes during RNA polymerase II transcription elongation. *Proceedings of the National Academy of Sciences of the United States of America*, *107*(4), 1678–83. http://doi.org/10.1073/pnas.0913559107

Ohno, R., Kadota, Y., Fujii, S., Sekine, M., Umeda, M., & Kuchitsu, K. (2011). Cryptogein-induced cell cycle arrest at G2 phase is associated with inhibition of cyclin-dependent kinases, suppression of expression of cell cycle-related genes and protein degradation in synchronized tobacco by-2 cells. *Plant and Cell Physiology*, *52*(5), 922–932. http://doi.org/10.1093/pcp/pcr042

Pascucci, B., Russo, M. T., Crescenzi, M., Bignami, M., & Dogliotti, E. (2005). The accumulation of MMS-induced single strand breaks in G1 phase is recombinogenic in DNA polymerase ?? defective mammalian cells. *Nucleic Acids Research*, *33*(1), 280–288. http://doi.org/10.1093/nar/gki168

Peters, J. W., Stowell, M. H., & Rees, D. C. (1996). A leucine-rich repeat variant with a novel repetitive protein structural motif. *Nature Structural Biology*, *3*(12), 991–994. http://doi.org/10.1038/nsb1296-991

Pfaffl, M. W., & Pfaffl, M. W. (2001). A new mathematical model for relative quantification in real-time RT-PCR. *Nucleic Acids Research*, *29*(9), e45. http://doi.org/10.1093/nar/29.9.e45

Prakash, S., & Prakash, L. (2000). Nucleotide excision repair in yeast. *Mutation Research/Fundamental and Molecular Mechanisms of Mutagenesis*, *451*(1-2), 13–24. http://doi.org/10.1016/S0027-5107(00)00037-3

Queimado, L., Rao, M., Schultz, R. A., Koonin, E. V, Aravind, L., Nardo, T., … Friedberg, E. C. (2001). Cloning the human and mouse MMS19 genes and functional complementation of a yeast mms19 deletion mutant, *29*(9), 1884–1891.

Reape, T. J., Molony, E. M., & McCabe, P. F. (2008). Programmed cell death in plants: Distinguishing between different modes. *Journal of Experimental Botany*, *59*(3), 435–444. http://doi.org/10.1093/jxb/erm258

Reinhold, H., Soyk, S., Simková, K., Hostettler, C., Marafino, J., Mainiero, S., … Zeeman, S. C. (2011). β-amylase-like proteins function as transcription factors in *Arabidopsis*, controlling shoot growth and development. *The Plant Cell*, *23*(4), 1391–1403. http://doi.org/10.1105/tpc.110.081950

Roth, C. M. (2002). Quantifying Gene Expression, 93–100.

Scofield, S., Jones, A., & Murray, J. a H. (2014). The plant cell cycle in context. *Journal of Experimental Botany*, *65*(10), 2557–2562. http://doi.org/10.1093/jxb/eru188

Seroz, T., Winkler, G. S., Auriol, J., Verhage, R. a, Vermeulen, W., Smit, B., … Hoeijmakers, J. H. (2000). Cloning of a human homolog of the yeast nucleotide excision repair gene MMS19 and interaction with transcription repair factor TFIIH via the XPB and XPD helicases. *Nucleic Acids Research*, *28*(22), 4506–4513.

Stehling, O., Vashisht, A. A., Mascarenhas, J., Jonsson, Z. O., Sharma, T., Netz, D. J. A., … Wohlschlegel, J. A. (2013). metabolism and genomic integrity, *337*(6091), 195–199. http://doi.org/10.1126/science.1219723.MMS19

Suesslin, C., & Ã, H. F. (2003). An *Arabidopsis* mutant defective in UV-B light-mediated responses, 591–601.

Torabinejad, J., & Caldwell, M. M. (2000). Inheritance of UV-B Tolerance in Seven Ecotypes of *Arabidopsis* thaliana L . Heynh . and Their F 1 Hybrids, 228–233.

Upadhyaya, M. K., & Golaszewski, J. (2003). The effect of UV-B radiation on plant growth and development, *2003*(3), 135–140.

Van Wietmarschen, N., Moradian, A., Morin, G. B., Lansdorp, P. M., & Uringa, E. J. (2012). The mammalian proteins MMS19, MIP18, and ANT2 are involved in cytoplasmic iron-sulfur cluster protein assembly. *Journal of Biological Chemistry*, *287*(52), 43351–43358. http://doi.org/10.1074/jbc.M112.431270

Wan, K. H., Yu, C., George, R. A., Carlson, J. W., Roger, A., Svirskas, R., … Celniker, S. E. (n.d.). High-Throughput Plasmid cDNA Library Screening, *14*(Figure 1).

Zhou, X., Jin, Y., Yoo, C., & Lin, X. (2013). CYCLIN H; 1 Regulates Drought Stress Responses and Blue Light-Induced Stomatal Opening by Inhibiting Reactive Oxygen Species Accumulation in Arabidopsis. *Plant …*, *162*(June), 1030–1041. http://doi.org/10.1104/pp.113.215798

APPENDIX

APPENDIX

PRSV – Papaya ring spot virus, a disease that affects the leaves of papaya trees worldwide and has devastating effects on agricultural production.

SunUp – A transgenic cultivar of papaya that was produced by the Hawaii Agricultural Association during the early 1990's to be resistant against papaya ring spot virus.

F2 mapping – The name given to genetic mapping where a cross between two second generation offspring are bred together to produce a homozygotic recessive phenotype.

MMS19 – Methyl methane sulfonate, the name given to a carcinogenic chemical that induces severe lesions within DNA. Originally identified as a gene within yeast in the 1970's.

qPCR – (Real-time)Polymerase chain reaction where a thermal cycler and thermo labile DNA polymerase exponentially copy desired parts of a DNA or RNA strand. Can be used to quantify mRNA expression.

Hoechst stain – A blue fluorescent stain with an emission wavelength of 450 nm used for identification of nuclear material within a cell.

Pfaffl equation – A method used in molecular biology to quantify expression of mRNA using real-time PCR. Protocol requires the use of house-keeping genes and relative expression profiles.

TEM – Transmission electron microscopy, the field in which high resolution images are acquired through the use of fixing, dehydrating and embedding tissues in resin to be sectioned and viewed on a two dimensional screen.

SEM – Scanning electron microscopy, the field in which high resolution images are acquired through similar processes as TEM, but where gold particles coat a specimen so as to view three dimensional images using a computer program.

RAD – Radiation deficient genes originally identified in yeast screens where radiation knock outs exhibited increased susceptibility to DNA damage.

SSB – single strand breaks in DNA formed by a variety of factors such as UV-B radiation or stalled replication forks.

RNA Pol II – The enzyme necessary for transcribing most of the genes that produce functional proteins from DNA into pre-mRNA.

CPD – cyclobutane pyrimidine dimers are a form of photoproduct produced by UV-B radiation that distorts the double helix formation within DNA.

NER – Nucleotide excision repair, the process through which damaged DNA is excised and repaired using the anti-sense strand as a template. Repairs a large array of damaged forms of DNA.

In vitro – Latin for "grown in glass" when referencing tissue culture or bacterial cultures grown in glass petri dishes

TFIIH – Transcription factor II h, the large multiplex enzyme component of RNA Pol II that functions as the catalytic core and is involved in transcription initiation, elongation and nucleotide excision repair.

LRM – Leucine rich motifs, a structural motif that occurs within proteins where a repeating amino acid rich in hydrophobic leucine form a solenoid domain.

HEAT repeats – A solenoid protein domain that can be found in several cytoplasmic proteins. Originally named after the genes in which this LRM motif was identified. Heat repeats have been implicated in MMS19 domain function.

XPD/XPB – Xeroderma pigmentosum D/B, named after the disease diagnosed in individuals with mutated genes that prevent proper DNA repair from UV-B damage, inducing malignant melanomas at an alarming rate and ultimately death.

Fe-S clusters – Iron Sulfur clusters that are ubiquitous inorganic cofactors found within a variety of enzymes and proteins. Responsible for an array of metabolic and DNA directed functions within all organisms.

CIA pathway – Cytosolic iron sulfur cluster assembly; the pathway responsible for building these inorganic cofactors into necessary enzymes after they are released from the mitochondria into the cytosol.

TC-NER/GG-NER – The two forms of nucleotide excision repair that exist. Transcription coupled NER is an ongoing process throughout the cell's life cycle as genes are transcribed, any errors or distortions in the double helix are excised and repaired. Global genomic NER does not depend on transcriptionally active genes but instead targets any damaged sites within the genome through unique damage sensing proteins.

CSB – Cockayne syndrome group B protein that is important in remodeling chromatin structure during the global genomic repair process.

XPC – An NER protein that is associated with identifying the areas of damage within the genome during GG-NER.

UV-DDB – UV-damaged DNA-binding protein that is linked to the DNA damage sensing response.

CAK complex – The associated proteins that form the secondary part of TFIIH holoenzyme including Cdk-activating kinases

CDK7 – Cyclin-dependent kinase 7, a necessary component of the CAK complex within TFIIH. Implicated in maintaining proper cell cycle progression.

Cyclin-H – The acting cyclin that phosphorylates CDK7 so as to bind properly to the core TFIIH proteins. This enzyme has been implicated in expression of a drought tolerance phenotype in *Arabidopsis*.

BE – Base excision repair, a form of DNA repair that exists in both prokaryotes and eukaryotes.

HR – Homologous recombination, the method through which a eukaryotic cell is able to reduce the effect of damaged DNA by combining a sequence from a complimentary chromosome.

ATM/ATR – Ataxia telangiectasia mutated and Rad3 related. The two distinct signaling pathways that are used by the cell to alert DNA damage repair proteins to the presence of DNA damage.

BIOGRAPHICAL SKETCH

Jorge A. Trujillo was born in Hidalgo, Texas, United States of America on September 4, 1989. At the age of 1 his family moved to Morelia, Michoacán, Mexico where he would grow up for the next 5 years. After learning Spanish as his primary language, his family moved back to the US and has resided permanently in McAllen for the past 20 years. He would attend primary and secondary school in McAllen and then high school at The Science Academy in Mercedes where he would graduate in the top 25%.

In the fall of 2008 he would start his Bachelor of Science in pre-medicine and then transfer to a biology degree in 2009. He would graduate with a Bachelor of Science in Biology in the Fall of 2012 while starting his first semester in graduate school.

The Master of Science degree in Biology was pursued in the Fall of 2012 under the supervision of Dr. Anxiu Kuang, Dr. Qingyi Yu, Dr. Luis Materon and Dr. Richard Gilkerson. Throughout all of graduate school Jorge would be employed as a graduate assistant in teaching the 1401 biology labs (for two years) and then as an EM technician for both the biology and chemistry department. In the spring of 2013 Jorge would attend an internship at AgriLife Dallas that would continue through the entire summer. On July 2015, Jorge completed his Master's degree and is looking for employment in both the electron microscopic sciences and molecular biology. He currently resides at 7220 N. Bentsen Rd, McAllen TX with his family.